


# Towards an automated acquisition and parametrization of debris-flow prone torrent channel properties based on photogrammetric-derived uncrewed aerial vehicle data

Gregor Schmucki<sup>1,2,4</sup>  | Perry Bartelt<sup>1,2</sup> | Yves Bühler<sup>1,2</sup> | Andrin Caviezel<sup>1,2</sup> | Christoph Graf<sup>3</sup> | Mauro Marty<sup>3</sup> | Andreas Stoffel<sup>1,2</sup> | Christian Huggel<sup>4</sup>

<sup>1</sup>WSL Institute for Snow and Avalanche Research SLF, Davos, Switzerland

<sup>2</sup>Climate Change, Extremes, and Natural Hazards in Alpine Regions Research Center CERC, Davos, Switzerland

<sup>3</sup>Swiss Federal Institute for Forest, Snow and Landscape Research WSL, Birmensdorf, Switzerland

<sup>4</sup>Department of Geography, University of Zurich, Zurich, Switzerland

## Correspondence

Gregor Schmucki, WSL Institute for Snow and Avalanche Research SLF, Davos CH 7260, Switzerland.

Email: [gregor.schmucki@impulsthun.ch](mailto:gregor.schmucki@impulsthun.ch)

## Abstract

Debris flows are a hazard in mountainous regions. Cost-effective, long-term studies of debris-flow torrents, however, are rare, leading to uncertainties in hazard assessment and hazard prevention. Here, we address the question of whether cost-effective remote sensing techniques can be applied for assessment of mountain torrents and possibly further gather accurate, long-term information on the evolution of the catchment. Torrents prone to debris flows are often devoid of vegetation in the near channel area and hence can be well captured with photogrammetrically derived methods using uncrewed aerial vehicle (UAV) surveys. The possibility of automatically extracting specific torrent parameters from high-resolution terrain models, such as cross-section area or gradient, is investigated. The presented methodology yields continuous and automatically derived geometrical parameters such as torrent bed width, inclination and cross-section area, which is a major advantage compared with point-based, often dangerous field surveys. Their cross-validation with field measurements shows strong agreement. Those parameters are accurate along sharply incised sections with strong limitations along sections with steep adjacent slopes and/or dense vegetation. The information along the torrent allows fast identification of key sections and weak spots which can be precisely evaluated in the field. The study highlights that proper classification of real ground points poses the key challenge. We show that photogrammetric routines to derive a high-resolution digital terrain model (DTM) are limited in the case of dense vegetation coverage. In such cases, LiDAR surveys have clear advantages even though they are also limited by very dense vegetation. We find that UAV data can be used for an objective method of estimating debris-flow torrent geometric properties. And the introduced approaches therefore build a stepping stone towards a more comprehensive, reproducible and objective assessment of torrent processes and predispositions. However, ground-referencing fieldwork remains essential, and further research on remote sensing supported hazard assessment of debris-flow-prone torrents is indispensable.

## KEYWORDS

debris flows, GIS, hazard assessment, LiDAR, natural hazards, OBIA, photogrammetry, point cloud, UAV

This is an open access article under the terms of the [Creative Commons Attribution-NonCommercial-NoDerivs](https://creativecommons.org/licenses/by-nc-nd/4.0/) License, which permits use and distribution in any medium, provided the original work is properly cited, the use is non-commercial and no modifications or adaptations are made.

© 2023 The Authors. *Earth Surface Processes and Landforms* published by John Wiley & Sons Ltd.

## 1 | INTRODUCTION

Debris flows are gravitationally driven mass movements containing a mixture of rocky debris and water. Depending on the composition, they can reach high velocities ( $>10$  m/s), long runout distances up to several kilometres, and exert extreme pressures ( $>30$  kPa) on buildings and other constructions such as bridge abutments (Hürlimann et al., 2019). Debris flows are typically triggered by intense rainfall events and associated runoff processes. They are considered as one of the most unpredictable and destructive landslide processes known in mountain regions (Hungri et al., 2001; Iverson, 1997; Iverson et al., 2011; Jakob & Hungri, 2005; Takahashi, 2007). The damage tends to increase with the amount of sediment transported to the fan during an event, especially when water and sediment leave the channel (Rickenmann, 2014). This can lead to large inundated areas and widespread destruction. The accurate hazard assessment and planning of protective measures in torrent catchment areas for debris flows is therefore an important part of integral risk management of natural hazards in mountainous regions.

One of the fundamental difficulties in debris-flow mitigation is to determine debris-flow volumes and mixtures which control in large part the possible inundation area and the likelihood of channel out-breaks (Zubrycky et al., 2021). Hazard assessment methods are used by natural hazard experts to estimate both release and erosion volumes. However, the application of these methods is based strongly on engineering experience and often subjective to individual judgement (Berger et al., 2011; Jakob, 2021; Rickenmann, 2016).

Because debris-flow volumes are directly linked to the volume of available sediments within the torrent, field studies are highly important. Nonetheless, even field studies are hampered by the fact that they typically provide a present picture of the torrent state. It is absolutely necessary to understand how the torrent will evolve over time to accurately predict future debris-flow activities (Berger et al., 2011; de Haas et al., 2020). Debris-flow events are rare, in comparison with, for example, snow avalanches, which can occur every year at a specific site. The comparably low activity of debris-flow torrents implies that long-term monitoring of dangerous torrents is required but still seldom performed. Sediment accumulation rates must therefore be estimated by the hazard expert, with little or no long-term data because the disposition of sediments in the torrent is rarely quantified, or monitored over long time periods.

In this work, we investigate how photogrammetric drone flights can be used to improve accuracy and efficiency in torrent mapping, specifically to obtain continuous estimates of torrent parameters and hence potential debris-flow volumes. Repeated photogrammetric uncrewed aerial vehicle (UAV) flights allow characterizing the development of landforms over time (Adams et al., 2016; Cucchiari et al., 2018; de Haas et al., 2018; de Haas et al., 2020; Niculiță et al., 2020; Passalacqua et al., 2015; Walter et al., 2022). Based on available spatial data, numerical simulation models of debris flows can be further developed and their parameters determined with greater accuracy (Graf et al., 2019). Based on the derived high-resolution digital terrain model (DTM), we aim to systemically map debris-flow-prone torrents. However, the runout zones of debris flows are often densely vegetated (and sometimes densely populated or crossed by lifelines such as roads, railroads or energy transport systems). To properly capture the morphology of the landscape and the associated change over

time, the point cloud data obtained with UAVs must be classified into ground and nonground points. Here, we develop and test two classification algorithms for photogrammetric data. We automatically extract torrential properties, which could in the future also support hazard assessments. We focus mainly on geometrical parameters, which are conventionally extracted in the field during a geomorphological assessment of the torrent in a discrete and laborious manner. Further approaches, which may be applied within a UAV-based hazard assessment, such as geomorphological change detection are introduced and their limitations concerning the handling of systematic errors and occlusion effects are discussed.

The application of UAV-based data for torrent hazard assessment and mapping is beyond the scope of this study. Nevertheless, our study may indicate potential and limitations of UAV data to support and complement time and cost intensive field work in the context of hazard analysis, modelling and mapping.

## 2 | STUDY SITES

We selected two small test sites in the canton of Grisons (GR) in Switzerland in order to investigate how UAV can be applied for torrent assessment: Arelen (Davos, GR) and Fräschmardin (Klosters, GR). The Arelen and Fräschmardin catchments have similar sizes and represent highly diverging structures of the channel network and sediment supply chain as well as strongly differing lithologies. Both torrents extend beyond the tree line and thus have a vegetation-free upper catchment and a vegetated transit and runout zone (see Table 1). This makes them well suited to assess the UAV performance in vegetated and nonvegetated terrain. Frequent debris-flow events of several  $1000\text{ m}^3$  have been observed in the last couple of years within both

**TABLE 1** Overview of the main characteristics of the Arelen and Fräschmardin catchments.

	Arelen	Fräschmardin
Catchment area	0.8 km <sup>2</sup>	1.06 km <sup>2</sup>
Altitude	1638–2530 m a.s.l.	1294–2657 m a.s.l.
Length torrent (horizontal)	1.87 km	1.96 km
Length torrent (terrain)	2.0 km	2.18 km
Mean Sslope	31%	43%
Aspect	East	South
Melton (1965)	0.997	1.325
Geology	Ophiolite	Mönchalp Gneiss
Surface coverage	45% weathered rock 35% shrub forest 15% forest 5% grassland	30% grassland 25% rock 20% shrub forest 20% forest 5% weathered rock
Other processes	Avalanche, rockfall	Avalanche, rockfall
Constructions	Retention dam, check dams (partly damaged)	Embankment solidification, lateral dams



catchments (unpublished reports). Within field campaigns during summer 2020, the channel geometry and possible erosion rates were estimated for each subdivided section A–H, respectively A–G (see Figure 1). The distance measurements were taken with a TruPulse 360°B Laser Range Finder at a representative cross-section within the subdivided section. Erosion rates were estimated on-site according to the SEDEX method (Frick et al., 2008, 2011; Kienholz et al. 2010). The estimated measures of the torrent geometry we could later use to validate the automatic extraction of the torrential properties.

## 2.1 | Arelen

The Arelen torrent is located near Davos Wolfgang (see Figure 1) and is relatively active; a retention dam has been constructed in 2018 to protect the buildings located at the Wolfgang pass. The topography around the Wolfgang pass is shaped by three major rockslides from the Totalphorn (late pleistocene; about 400e6 m<sup>3</sup>) (Abele, 1974; Maisch, 1981; Signer et al., 2018). The geology of Davos Arelen is dominated by strongly tectonized and weathered ophiolites. During heavy rainfall, water can hardly infiltrate because the underlying rock is less permeable than the loose surface. Roughly estimated field based erosion rates per classified sections suggest that unconsolidated sediments can easily be mobilized by debris flows of several 1000 m<sup>3</sup>. The numerous channels build a complex network. Recently observed debris-flow events were characterized by several surges within short succession and a high water content

(unpublished reports). The morphology of the torrent cone is characterized by repetitive patterns, which express the occurrence of many smaller debris-flow events. The catchment provides a quasi-unlimited supply of sediments. The highly weathered ophiolite is capable to store relatively large amounts of water from precipitation. The high antecedent moisture of the soil has a major influence on both, the likelihood and erodibility of a debris-flow event. The size of the event is mainly limited by the intensity and duration of the precipitation event. Because the catchment size of 0.8 km<sup>2</sup> is relatively small, the expected runoff is also low. We can observe that the current position of the fan apex is in the middle of the debris cone. Current events tend to be erosive in the upper part of the cone and deposit material along the lower part. As can be seen clearly in Figure 1, the retention dam was built assuming that events leave the torrent no further up than the actual cone apex.

Based on field inspections we have assessed a specific debris-flow volume for an event with a frequent (1–30 years) to average (30–100 years) return period with the numerical values based on (BAFU, 1997). Above the major confluence, an erosion volume of 2500 m<sup>3</sup> is estimated, whereby the major part originates from the orographic right subcatchment. An average erosion rate of 3 m<sup>3</sup>/m is estimated between the confluence and the actual fan apex. This sums up to an expected debris-flow volume of 4500 m<sup>3</sup> if both subcatchments are active. Along the remaining lower part (sections A–C), we do not expect significant erosion rates, as the torrent inclination decreases.

Based on technical reports and event documentation (unpublished reports) prepared for the planning phase of the retention

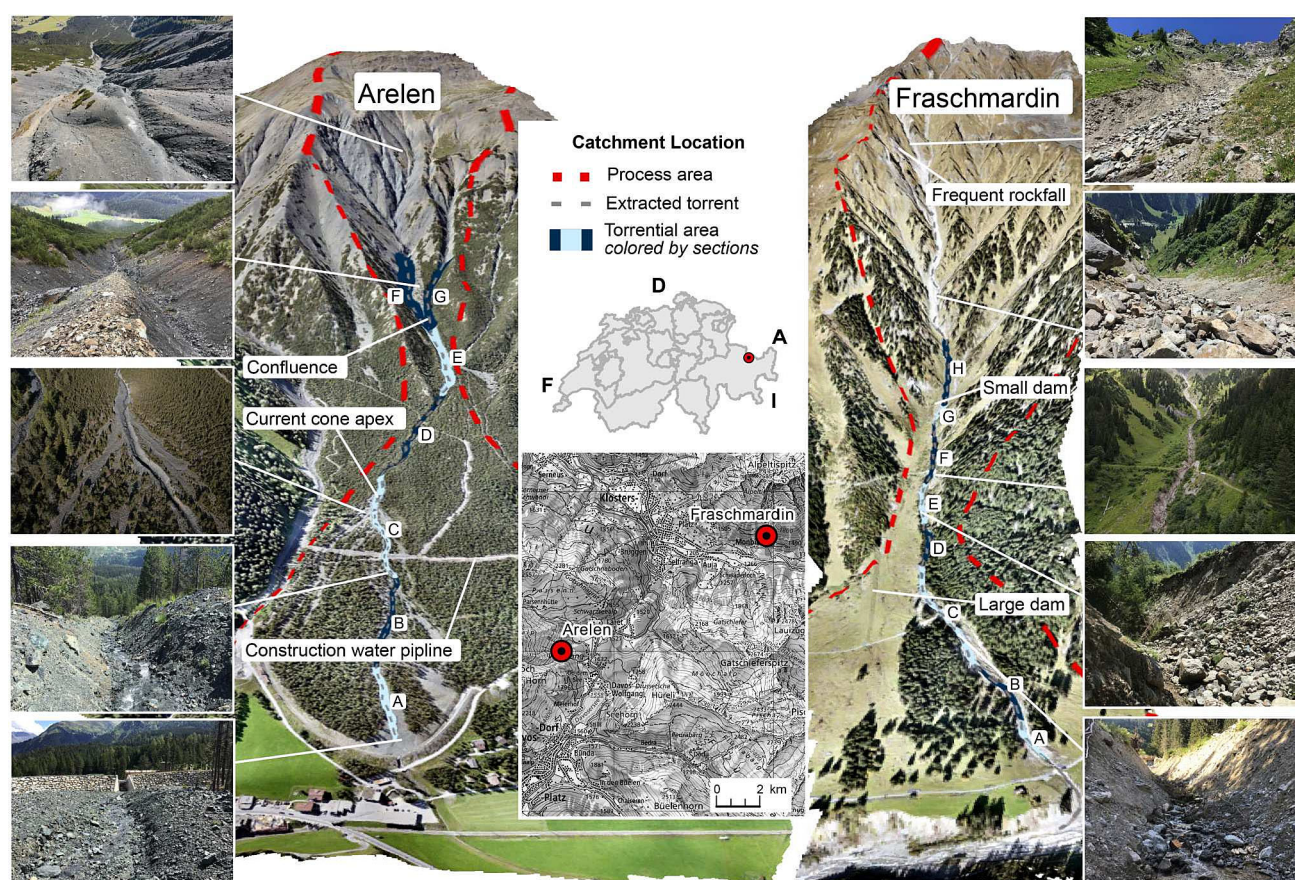


**FIGURE 1** Overview of the two main study sites Arelen (left) and Fräschmardin (right). The torrential area is visualized in blue, the sections are coloured in light and dark blue. The red dashed line indicates the catchment area, representing the upper watershed and the entire fan apex. The various insets highlight specific catchment locations [Color figure can be viewed at [wileyonlinelibrary.com](https://onlinelibrary.wiley.com/doi/10.1002/esp.5585)]

dam, we expect a volume of 3000–5000 m<sup>3</sup> for an event with a frequent to average return period. Due to the limitations of the catchment size, we do not expect events with rare (100–300 years) or very rare (>300 years) return periods to be of a significantly greater magnitude. Magnitude estimates of other technical reports vary largely, however in the Swiss federal event StorMe (BAFU, 2019), where events with damaging effects on infrastructure are recorded, no larger volume than 4000 m<sup>3</sup> is documented.

## 2.2 | Fraschmardin

The second study site, Fraschmardin, has an area of 1.06 km<sup>2</sup>. The lithology consists of Mönchalp Augengneis. The rock mechanical properties of this gneiss lead to a grain size distribution that is dominated by large boulders originating from the rockfall-prone head wall at 2600 m a.s.l. There is one main channel leading from the headwall down to the Landquart river. From field investigations, we expect one main debris-flow surge to be decisive for the resulting magnitude, this is in accordance with technical reports and event documentation (unpublished reports). The morphology of the torrent changes with elevation. Along the uppermost part of the catchment, frequent rockfall activity leads to an unlimited supply of debris. Fresh, not yet weathered surfaces indicate recent activity. Beyond 1800 m a.s.l. elevation, the torrent is clearly incised. The estimated erosion volume varies between 2–3 m<sup>3</sup>/m. Along the middle part (around 1500 m a.s.l.) landslide processes add an additional volume of 300 m<sup>3</sup>. Frequent to average debris-flow events will follow the torrent and only mobilize minor parts of the available debris stored in the uppermost catchment, with an estimated erosion volume of ~7000 m<sup>3</sup>. Summing all these quantities, we reach an expected debris-flow volume of 10 000 m<sup>3</sup> for frequent to average events. The rough morphology of the cone indicates the occurrence of large events which have threatened the hamlet Monbiel in the past. At the fan apex, where a small dam is constructed (see Figure 1), we expect rare events to be significantly larger and have the potential to leave the torrent. If the initial debris flow can transport larger volumes, the erosion volume downstream and the probability of breakout increases, especially in the narrow bends and near the damaged structures.

## 3 | METHODS

### 3.1 | UAV surveying

The amount of UAV-based research has increased enormously in the last decades and has become accessible to the public. UAVs can be equipped with cameras, temperature sensors, LiDARs and many other measurement tools. Applications range from monitoring to mapping, search and rescue and much more (Giordan et al., 2018).

Three different UAV categories can be differentiated: vertical takeoff and landing (VTOL), rotary-wing systems, such as helicopters and multirotor platforms, and thirdly fixed-wing systems (Ducard & Allenspach, 2021). The most common are multirotor UAVs with four or more propellers. They have the capability to hover and are able to carry relatively heavy payloads. Fixed-wing UAVs have the advantage to fly over large distances and capturing large areas. Hybrid flying platforms such as the fixed-wing hybrid VTOL UAV (e.g., WingtraOne) combine the

advantage of long flight duration time of fixed-wing with VTOL capabilities coming from multirotor systems (Ducard & Allenspach, 2021).

UAVs that are equipped with real-time kinematic (RTK) or post-processed kinematic (PPK) technology introduce the advantage that ground control points (GCP) are not indispensably needed (Zhang et al., 2019). Checkpoints (CPs) can assess the achieved geolocation accuracy of the resulting DSM, DTM and orthophoto. Table 2 shows the specifications of the different platforms used.

The tailsitter VTOL WingtraOne is able to take off, transit and land autonomously. With the WingtraOne, it is possible to complete high-precision aerial surveys and mapping tasks. The high-end camera set-up (42 MP Sony RX1R II) enables precise imaging even at high altitudes. We used the Sony RX1R II camera with a 42 MP full-frame sensor and a 35 mm lens. We applied the Wingtra standard settings with a shutter speed of 1/2000 s and an aperture of 4 resulting in ISO values of 100–800. Unfortunately, the company Wingtra does not provide detailed information on its GNSS and IMU modules (Wingtra, 2022). To process the GNSS data, we applied reference measurements from the Swiss AGNES network (AGNES, 2022), using the Station Davos with a distance of 2.5 km to the investigation area Arelen and 9 km to the site Fraschmardin.

The image position is postprocessed with PPK. The DJI Matrice 600 Pro is a professional UAV. We have mounted a RIEGL miniVUX-3UAV airborne laser scanner, which is a high-precision laser operating at 300 kHz with a field of view of 120°, resulting in a dense point pattern on the ground. The resulting point density varies with the flight altitude and pattern. Different scanner configurations with respect to lines per second and scan repetition rates are used depending on the operating velocity and altitude. The scanner is extremely light and compact (1.5 kg) and stores up to five target echoes per laser shot. Internal IMU and GNSS enable PPK positioning with centimetre accuracy.

### 3.2 | Data acquisition

Good weather conditions, that is, no strong winds (>10 m/s), fog, precipitation or harsh sun/shadow contrasts, are a prerequisite for successful data acquisition. The two catchments presented here in more detail are both flown with the WingtraOne. The flight planning was done on a tablet and performed with the proprietary WingtraPilot software. We flew with an image overlap of 80% along the track and 60% across the

**TABLE 2** Technical specification table of used UAVs.

Name	WingtraOne	DJI Matrice 600 Pro with RIEGL miniVUX-3UAV
UAV type	Tailsitter VTOL	Hexacopter
Weight	4.3 kg	10 kg
Maximum payload weight	800 g	5.5 kg
Battery capacity	198 Wh	780 Wh
Maximum flight speed	16 m/s	18 m/s
Wind resistance	12 m/s	8 m/s
Sensor	42 MP Sony RX1R II	Riegl miniVUX-3UAV
Location service	PPK	PPK
Price	~35 000 CHF	~150 000 CHF



track and an average flight altitude of 200 m above ground, resulting in an average ground sampling distance (GSD) of ~3 cm.

We performed further reference flights using the DJI M600 pro equipped with a Riegl miniVUX-3UAV LiDAR in order to compare the quality of photogrammetric-derived DTMs in the Arelen catchment in relation to LiDAR-based DTMs. Here, the flight planning was done with the commercial UgCS (Version 4.2.156) suite.

### 3.3 | Data processing

After the flight, the geographical position of the WingtraOne UAV had to be postprocessed with WingtraHub (PPK). The Wingtra raw GNSS measurements were compared with raw measurements from a reference base station of the Swiss AGNES network (AGNES, 2022) and high-precision geolocation is calculated for each image. Further, we processed the images with Agisoft Metashape (Version 1.6.5.11249). The stand-alone software Metashape is based on Structure-from-Motion Photogrammetry (Koenderink & van Doorn, 1991; Verhoeven, 2011; Westoby et al., 2012) and provides a complete photogrammetric workflow. Camera calibration parameters were estimated with the standard routine of Agisoft.

A major deviation of the standard workflow includes the removal of uncertain tie-points (*projection error* >0.4; *reconstruction uncertainty* >10) of the sparse point cloud with gradual selection. We applied the settings *high quality* and *aggressive* depth filtering as proposed by Bühler et al. (2016) for the dense cloud processing. The management of systematic errors is not further elaborated, as we do not present geomorphological change detection applications within this study. Georeferencing for the LiDAR flights is achieved via postprocessing procedures with proprietary Applanix and Riegl software solutions POSPac (v8.6) and Riprocess 1.8.7.

### 3.4 | Ground classification of LiDAR point clouds

The LiDAR point clouds were classified with the Software LAsTools using the module *lasground new*, serving as comparison data sets. A *step size* of 3 m for the initial ground point detection was found to be working best for the classification of shrub forest the most challenging landcover type due to its medium sized but diffused vegetation cover. We processed two flight categories to analyse the effect on the resulting DTM quality: A dense double flight plan grid with lateral spacing of 50 m and a coarse single grid with lateral spacing of 120 m.

### 3.5 | Ground classification of photogrammetric point clouds

We have tested different ground classification routines in the scope of this work. Many conventional algorithms do not perform well with photogrammetric data, as they were developed using LiDAR data, which is able to penetrate through dense vegetation and provide the last return value close to the real ground. The best results with photogrammetric-based data were obtained by combining RGB and a LiDAR-based classification routine (Anders et al., 2019).

To be able to classify vegetation along photogrammetrically derived point clouds of steep alpine terrain, we have developed two RGB-based routines, deploying Terrasolid (Approach A) and LAsTools (Approach B), as depicted in Figure 2. Approach A starts by removing the least reliable, noisy and isolated points from the original point cloud (Figure 2b). Subsequently, a smoothed surface is generated, a vegetation index is generated and ground points are classified and extracted (Figure 2c–f). Approach B relies on a previously generated, officially available surface model. Hence, the first step is the calculation of the height difference to this reference height model (Figure 2h). This step is followed by the generation of the vegetation index and the identification of potential ground points as nongreen points and green points with less than 25 cm difference to the reference height model (Figure 2h,i). A two-step ground point classification on fine and coarse grid sizes for robust outlier filtering is performed and final ground points are classified in a final step (Figure 2j–l). The individual and detailed command sequences for both routines are found in Appendix A.

#### 3.5.1 | Approach A details: Point cloud classification with terrasolid

TerraScan is a powerful software solution for processing laser scanning point clouds (Terrasolid, 2021). Here, we aimed for a classification routine via the generation of a smooth surface, which then can be classified disregarding remaining noise (see Figure 3). In the first step, low reliability, noisy and isolated points were removed (see Figure 2b). All points were sorted by x and y. Points with low reliability were removed. The definition of high and low reliability relies on the confidence parameter of Agisoft and a proprietary Terrascan metric. According to TerraScan, points have to feature a *high average reliability* (>10) in a sphere of 0.5 m and its reliability value difference needs to be at least 40% of the average reliability value within the sphere of 0.5 m. A deep dive into the reliability metrics might be necessary for future developments. Isolated and 'low noise'—below the actual surface—were deleted: If a point within groups of ≤15 points was more than 0.4 m vertically lower, but still within a 2 m radius along xy plane to others, it was classified as a low point. If there were less than 15 points within a range of 3 m, points were considered isolated.

A smoothed surface was generated, which was used for the subsequent ground classification (see Figure 2c). Potential surface points that fit locally smooth surfaces within a sphere of 5 cm were extracted. Points with high reliability were weighted more heavily. The potential surface points were smoothed along xyz. Twenty-five to 30 neighbouring points were used to fit a second-degree surface, whereby the maximum displacement of a point in any direction is 20 cm. Areas of high density were thinned out; for a volume of 7 by 7 by 7 cm, one central point was kept. Once again low and isolated points were removed. Points within groups of ≤10 points that were more than 0.4 m vertically lower than the others, but still within a 1.5 m radius along xy plane to others, were treated as low points. If there were less than 15 points within 2 m, they were considered as isolated (see Figure 2c).

The generated smoothed surface was used for the ground classification routine (see Figure 2d–f). A vegetation index based on the RGB information of the points is calculated to optimise the ground classification algorithm:  $(2 \cdot G - R - B) / (2 \cdot G + R + B)$  (Terrasolid, 2021). The values of this normalized vegetation index lie in the interval [−1,1].

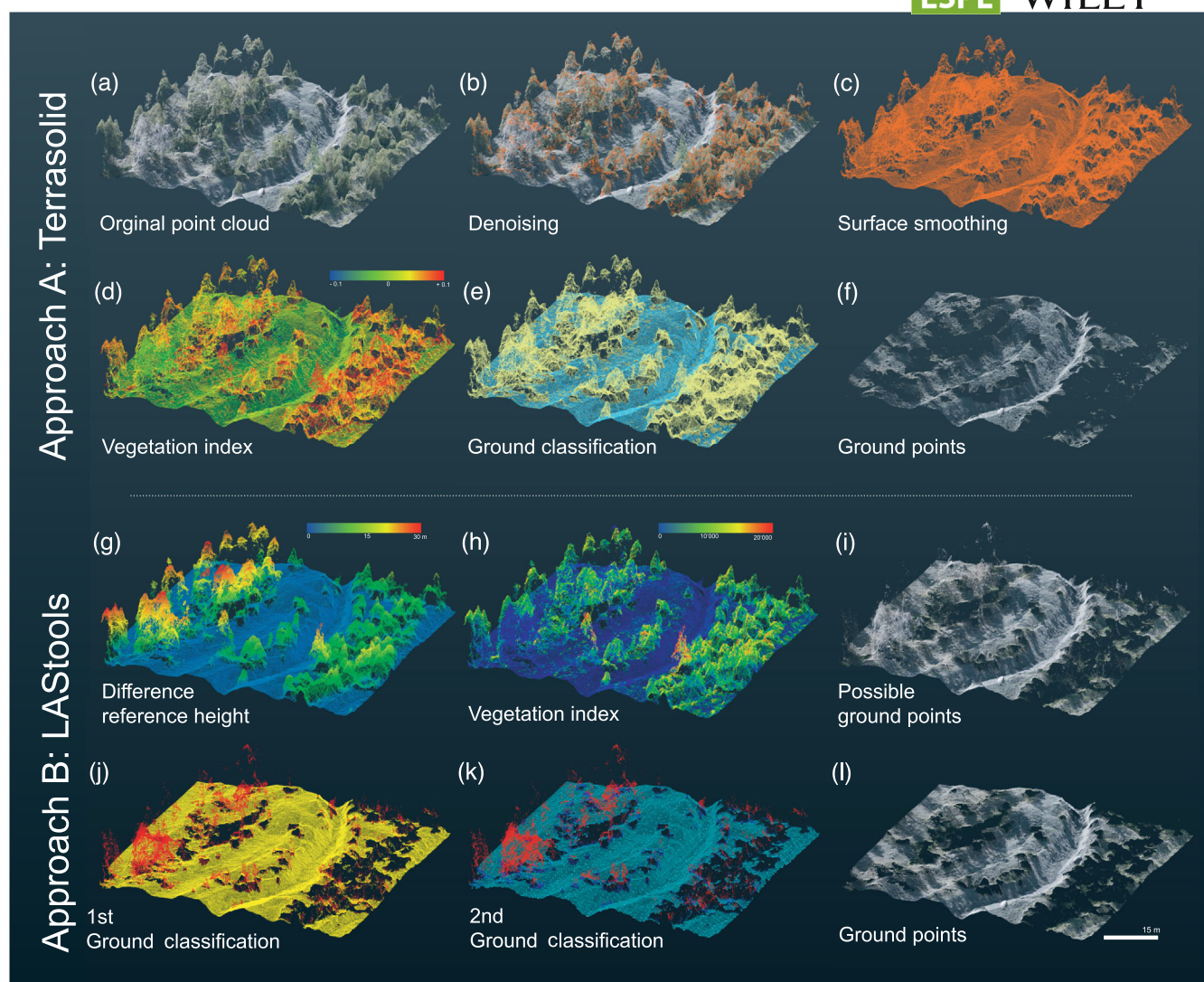


**FIGURE 2** Terrasolid and LAsTools workflows at an example area of the Arelen catchment. (a) Original point cloud. (b) Least reliable, noisy and isolated points are removed. (c) A smoothed surface is generated for the subsequent ground classification. (d) Generation of vegetation index. (e) Ground classification. (f) Final classified ground points. (g) Calculation of height difference to reference height model. (h) Generation of vegetation index. (i) Potential ground points identified as nongreen points and green points with less than 25 cm difference to the reference height model. (j) First ground classification with step size 1 m. (k) Second ground classification on the tapered ground with step size 6 m and noise filtering and removal of all points 6 m above reference height model and 1 m above first ground classification. (l) Final classified ground points. [Color figure can be viewed at [wileyonlinelibrary.com](https://onlinelibrary.wiley.com/doi/10.1002/esp.5585)]

Values above 0.05 were identified as green and thus likely to be vegetation. The aggregated colours were then smoothed by averaging the colour value by its nearest neighbours (average over a maximum of 10 points within a radius of 15 cm). We expected a maximum distance of any ground point of 60 m. A maximum permissible terrain angle of 75° and an iteration angle of 15 as classification maxima were chosen. The maximum distance of a point to the triangle plane was set to 1 m. The iteration angle was reduced if the edge length was smaller than 8 m (Terrasolid, 2021). The specific Terrasolid commands are found in Appendix A.

### 3.5.2 | Approach B details: Point cloud classification with LAsTools

LAsTools is a dedicated software instrument LiDAR point cloud post-processing, allowing us to customize the workflow to our specific needs. We aimed for a ground classification taking into consideration

all potential ground points, even below the uppermost vegetation layer, which is applicable in steep, densely vegetated terrain (LAsTools, 2022).

The algorithm is based on a colour classification, a reference height model and repeated TIN densification (see Figure 4). The degree of green is defined by the vegetation index  $2 \cdot G - R - B$  (Anders et al., 2019) (see Figure 2h). To be able to differentiate between grass and higher vegetation in steep terrain, we used a reference terrain model from Swisstopo (e.g., SwissSURFACE3D Swisstopo, 2022b) (see Figure 2g). For further processing we selected suited ground points: (i) nongreen points and (ii) green points within 20 cm, the uncertainty of the reference height model. A drawback is the remaining of dark points in the shade of high vegetation. We applied repeated TIN densification routines using various step sizes to reduce those artefacts within the unfiltered ground points.

A first ground classification with a step size of 1 m was performed (see Figure 2j). A thinning algorithm was applied to obtain the lowest

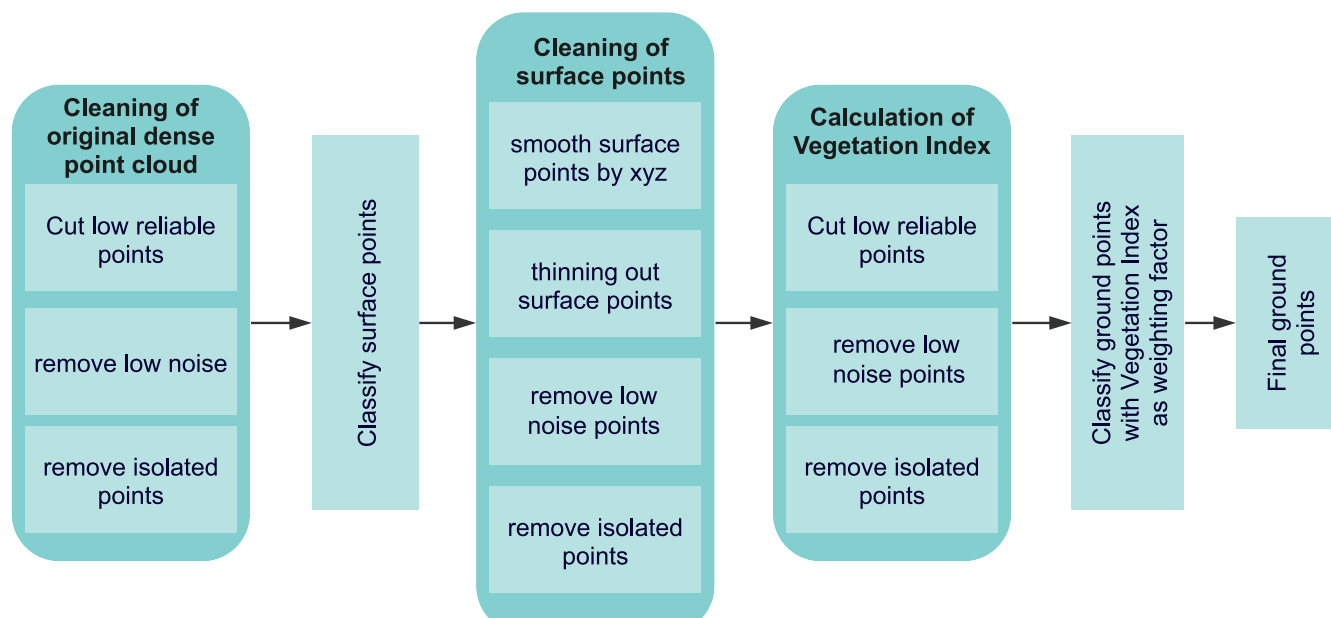


**FIGURE 3** Flowchart illustrating the workflow of the Terrasolid approach. The data preprocessing is based on three packages: (i) cleaning of the original point cloud, (ii) classification and cleaning of surface points and (iii) calculation of a smoothed vegetation index. Subsequently, the final ground classification is performed [Color figure can be viewed at [wileyonlinelibrary.com](https://onlinelibrary.wiley.com/doi/10.1002/esp.5585)]

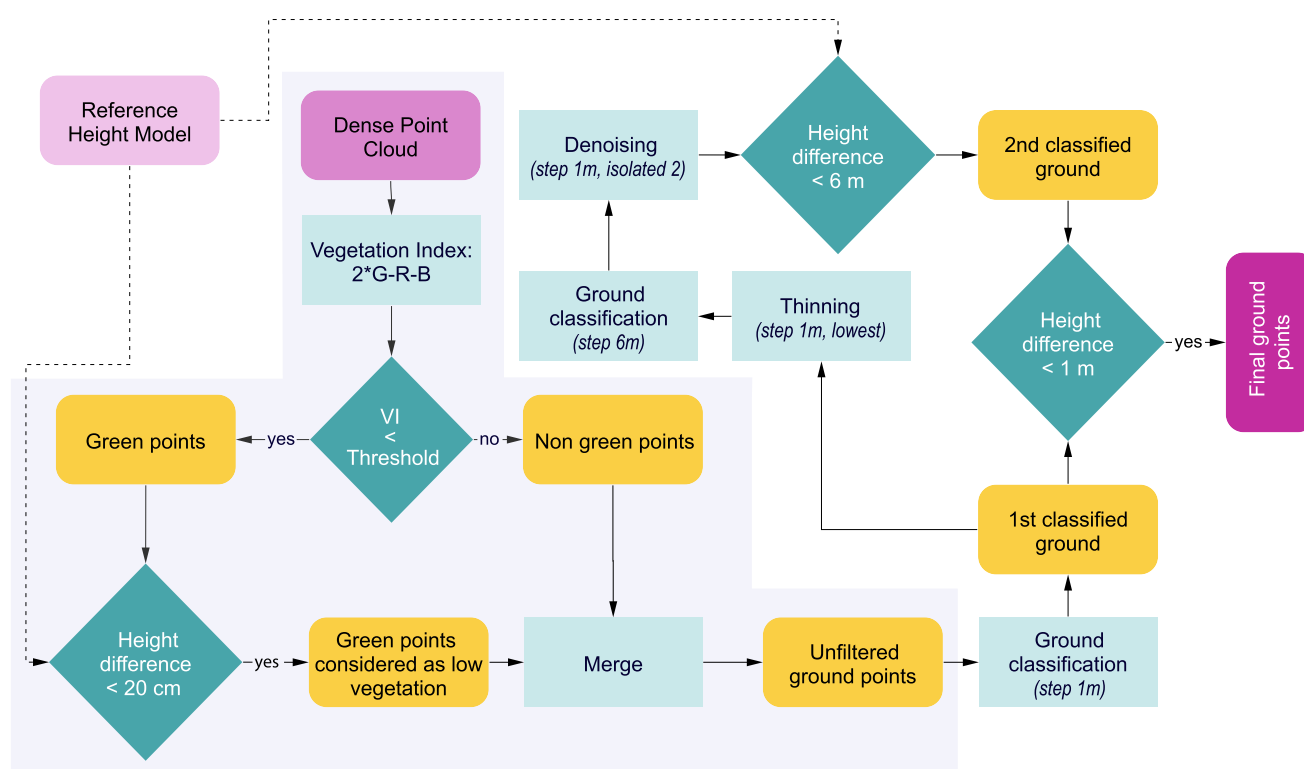


**FIGURE 4** Flowchart illustrating the workflow of the LAsTools routine. In the first step, the potential ground points (low vegetation and bare ground) are selected (greyed background). In subsequent iterative TIN densification with different step sizes, remaining noise points are removed [Color figure can be viewed at [wileyonlinelibrary.com](https://onlinelibrary.wiley.com/doi/10.1002/esp.5585)]

point within an area of  $1 \text{ m}^2$ . A second, coarser ground classification with a step size of  $6 \text{ m}$  was applied upon this thinned ground and a noise detection algorithm deletes points if there were less than 2 points in  $1 \text{ m}^3$ . Further, we calculated afresh a height deviation to the reference height model: All point clusters that had a larger distance than  $6 \text{ m}$  to the reference model, such as shadowy parts of trees, were deleted.

In a final calculation step, the difference between the first and the second rough ground classification was calculated. All points from the first classification that was more than  $1 \text{ m}$  above the second coarse classification (red points in Figure 2k) were deleted. The remaining points from the first ground classification (yellow points in Figure 2j) were then finally considered as ground points (LAsTools, 2022). All threshold values were determined empirically.



Once the ground points have been classified, the point cloud was rasterized into a DTM with a 10 cm grid spacing. The resulting high-resolution DTM could then be further used in various processing steps of the hazard assessment, for example, for the automatic extraction of torrential properties. The specific LAStools commands are found in Appendix A.

### 3.6 | Automated acquisition and parametrization of debris-flow prone torrent channel properties

For geomorphological assessments, an automatic morphological characterization of the torrent geometry allows for a more objective torrent analysis (Walter et al., 2022). We delineated the torrent bed, further segmented the adjacent embankments within the object-based image analysis (OBIA) software eCognition, and finally extracted the torrential properties by transects. We additionally estimated geometric torrential properties in the field to corroborate the

automatic approach. Here, we focus only on the key elements, a detailed description can be found in Schmucki (2022).

The Terrasolid derived DTM was sampled to a resolution of 25 cm and smoothed with a 3-pixel neighbourhood mean filter. Sinks were removed and derivatives such as flow direction and accumulation were calculated. After iterative testing, we decided to consider cells with flow accumulation values greater than 40 000 as torrents. However, this threshold value is highly dependent on the stream network characteristics of the catchment. The extracted torrent polyline was smoothed with the Polynomial Approximation with Exponential Kernel (PAEK) algorithm with a floating path of 10 m length in order to calculate representative cross-sections (see Figure 5). Transects with a width of 100 m—large enough to cover the whole torrential extent are generated perpendicular to the smoothed polyline each 0.5 m, densely enough to describe the cross-section geometry continuously along the torrent. Measurement of the channel depth for each transect was extracted and assigned to the respective transect line.

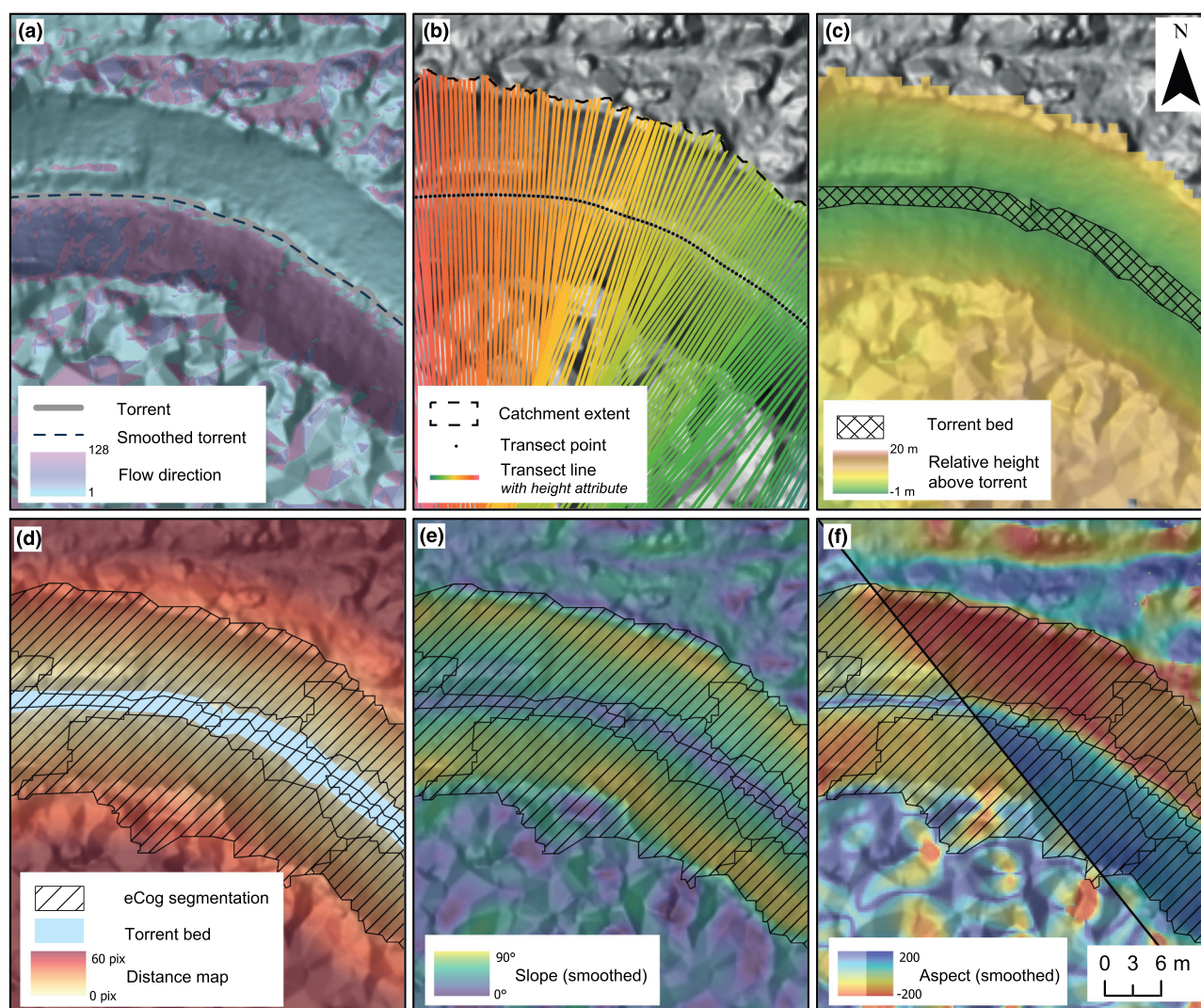


**FIGURE 5** Extraction of torrent bed and input parameter which are used to run the eCognition segmentation. (a) The torrent was extracted and smoothed based on a standard hydrology workflow applied on a smoothed DTM. (b) A transect line (100 m length) was generated every 0.5 m and clipped to the catchment extent. (c) The transect lines are rasterized based on the height attribute and subtracted from the DTM. A condition of less than 25 cm relative height above the torrent defines the torrent bed area. (d) A distance map representing the distance to the torrent bed was calculated in eCognition. The hatched surface indicates the resulting segmented torrential area. (e) The slope was directly derived from the smoothed DTM. (f) The two aspects are reclassified, such that they continuously represent the aspect [Color figure can be viewed at [wileyonlinelibrary.com](https://onlinelibrary.wiley.com)]



A major difficulty was to accurately map the confluence of different torrents. Because the transects have a width of 100 m, they interact with the neighbouring torrent channel, which likely has a different elevation. The confluence situation is shown in Figure 6a at the example of the Arelen torrent. The torrent in subcatchment I has a higher elevation than the torrent in subcatchment II and would therefore influence the torrent bed extraction of the torrent bed in subcatchment II. To counteract this problem, each section had to be calculated separately within the domain of its watershed. However, this effect will later distort the embankment calculation at the confluence. The identification of unique subcatchment pour points required a two-step approach ensuring the selection of the respective catchment branches. It consists of the determination of the potential pour point slightly upstream in the subcatchment branches and a subsequent radial search for the effective lowest point in the area of the potential pour point (Figure 6a/b). Finally, the transects are clipped to the extent of the catchment.

The clipped transect lines with an iso-spacing of 0.5 m along the smoothed torrent polyline were then rasterized with the height attribute on a resolution of 1 m in order to yield a continuous height attribute along the torrent. The relative elevation above the torrent bed was calculated from the difference between rasterized transect resampled to 25 cm and the DTM. We set the difference height

threshold to 25 cm below which we assign the torrent bed polygon. Across all sections, the polygons were joined and smoothed with the GIS *retain effective area* function of 1 m. An intersection selection with the smoothed polyline assures the selection of polygons representing the torrent bed. An aggregation of 2 m interconnects the polygons at the confluence.

Based on slope and aspect derived from the high-resolution DTM and a distance map, which quantifies the distance to the torrent bed, we run a multiresolution segmentation and generated objects with similar properties within eCognition (Trimble, 2022) (see Figure 5 and Table B1). Further, we automatically classified objects representing the torrential extent (see Figure 5 and Table B2). The classified torrential extent and the torrent bed polygon were used within a Python script to extract torrential properties. Transect feature classes from all sections were clipped by the torrential extent and joined to a common feature class. Points were generated every 25 cm along the generated transect lines and the elevation values from the DTM were stored as an attribute. The maximum transect provides information on how many transects were within a section. The points from the median transect line were used to identify the right and left embankment polygon according to their order. Dedicated clipping and buffering routines ensured accurate embankment assignments in boundary regions. For each section, the points representing all the transect lines

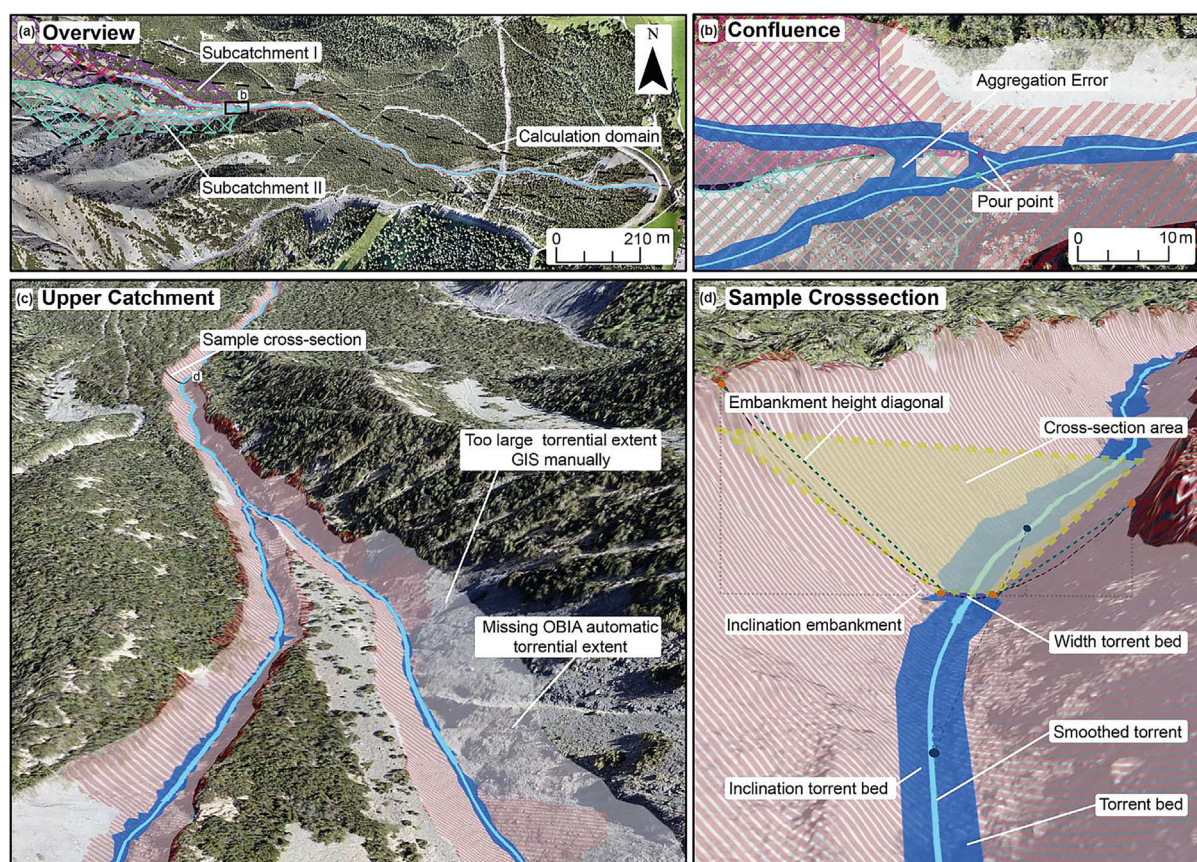


**FIGURE 6** (a) The catchment areas are used to limit the calculation domain to prevent interaction with the neighbouring subcatchment. This leads to calculation errors at the confluence. (b) Overview of the calculation domain. (c) All torrential properties are calculated every 0.5 m based on the torrent bed and the embankment polygons. The cross-section area is a trapezoid surface, considering the mean of both embankment heights. The inclination of the torrent bed was calculated based on a 10 m horizontal distance. The OBIA-based classification was partly limited due to triangulated DTM surfaces caused by dense vegetation. (d) In the upper catchment the classification of the embankments was limited by steep adjacent slopes [Color figure can be viewed at [wileyonlinelibrary.com](https://onlinelibrary.wiley.com/doi/10.1002/esp.5585)]

**TABLE 3** Overview of error measures of UAV flight with WingtraOne in the Arelen catchment.

Overall error	x-error	y-error	z-error	Yaw error	Pitch error	Roll error	Camera location error
0.084 m	0.0223 m	0.0535 m	0.0608 m	1.59°	1.12°	0.92°	0.038 m

were clipped by polygons (embankment left, embankment right, torrent bed) to derive their respective torrential properties, especially field-verifiable parameters such as torrent bed width and its inclination or the diagonal embankment height. Based on the properties of the torrent bed and the two embankment sides the cross-section area was derived (see Figure 6c).

## 4 | RESULTS

### 4.1 | Accuracy of SfM-processing

We validated our accuracy of our UAV flight with the WingtraOne on the 25 August 2021 based on 36 CPs regularly distributed over the Arelen catchment. We derived an overall accuracy of 0.084 m. Further accuracy measures of this flight mission can be found in Table 3 (Schmucki, 2022).

### 4.2 | Quality of different UAV-based DTMs

We developed two methodologies to classify nonvegetated ground points: Approach A based on Terrasolid and Approach B based on LAsTools. We compare the resulting photogrammetric ground classification of the two routines and relate them to LiDAR UAV acquisition with the DJI Matrice 600 Pro and Swisstopo product swissSURFACE3D (Swisstopo, 2022b). The latter captures all natural and human-made objects of the surface in the form of a classified point cloud. The minimum guaranteed ground point density is 5 points/m<sup>2</sup>, and the average ground point density is 15–20 points/m<sup>2</sup>. The planimetric accuracy is  $\pm 20$  cm and the altimetric accuracy is  $\pm 10$  cm. For the subsequent analysis, all classified ground points are rasterized to a 10 cm resolution DTM. We further compare the elevation with the preceding Swiss standard DTM swissALTI3D (Swisstopo, 2022a) with a spatial resolution of 2 m which is widely used for hazard analysis applications. It has to be noted that the swissALTI3D product continuously gets updated and the data of the swissSURFACE3D will be incorporated into this terrain model in the coming years. However, the low update frequency of about 6 years of the Swisstopo products will remain the main disadvantage compared to UAV-based derivatives. For other regions in the world, UAV-based terrain models are likely to be the only possibility to acquire a DTM with a submeter resolution, acceptable for the extraction of torrential properties and simulation applications.

The hillshades in Figure 7 highlight the advantages and disadvantages of the two routines. As Approach B uses a reference height model, grass and higher vegetation can be differentiated reliably. However, the remaining nongreen points needed to be eliminated with a coarse and aggressive noise removal algorithm. Steep rocky and artificial surfaces are therefore not accurately preserved. This effect is less pronounced in Approach A.

#### 4.2.1 | Elevation comparison

The elevation of the ground points was evaluated in relation to the 10 cm rasterized swissSURFACE3D data (see Figure 8).

In open forest areas, the interquartile range of the differences amounts to about  $\pm 20$  cm along all-terrain models. In the torrential area, the deviation from swissSURFACE3D is marginal for the UAV-based models (interquartile range  $\pm 10$  cm). The old swissALTI3D data reveal the limitations of a coarse and not up-to-date DTM. The median value of the high-resolution LiDAR UAV is closer to the swissSURFACE3D data compared with the low-resolution LiDAR for all investigated land surface types.

We can conclude that in open terrain such as torrents and open forests, the quality of photogrammetric data provides the same accuracy as the LiDAR UAV data; hence, photogrammetric data can be considered as sufficiently accurate to characterize the torrent geometry. Along densely vegetated terrain, the two photogrammetric algorithms are severely limited.

#### 4.2.2 | Ground point density

The ground point density describes the number of points classified as ground per square metre visualized in Figure 8 for shrub forests, open forests and torrent areas. Across all types of point cloud generation, we observe low point densities within shrub forest areas. However, the calculated point density does not serve as a direct quality measure, as classified ground points not necessarily are true ground points (see Figure 9). When analysing the ground point densities, it is important to consider the different data sources. The two photogrammetry datasets are from the same data source, and the difference in point density and accuracy in ground identification is the result of the different classification algorithms. The two UAV LiDAR datasets use the same processing, but the data were acquired in different ways, resulting in the differences in point density. The difference between the old swissALTI3D dataset and the SwissSURFACE3D reference data is greatest in the torrent areas, suggesting that the difference may be due to the low temporal and spatial resolution of the swissALTI3D dataset.

From Figure 8, we anticipate that photogrammetrically derived ground points are  $1.4 \pm 0.5$  m higher than the ground points of swissSURFACE3D in shrub forest. LiDAR UAV-derived point clouds tend to have a much higher ground point density along vegetated terrain. In shrub forests, the ground point densities of the photogrammetric-derived Terrasolid and LAsTools routine are very similar. In the open forest, we observe large variations: The LAsTools routine indicates a ground point density of various hundred points/m<sup>2</sup>, whereas the median ground point density along the Terrasolid routine is below 10 points/m<sup>2</sup>. Below trees, we find no ground points in either routine. However, in the open areas between trees, the ground point density of the LAsTools routine is similarly high as along the



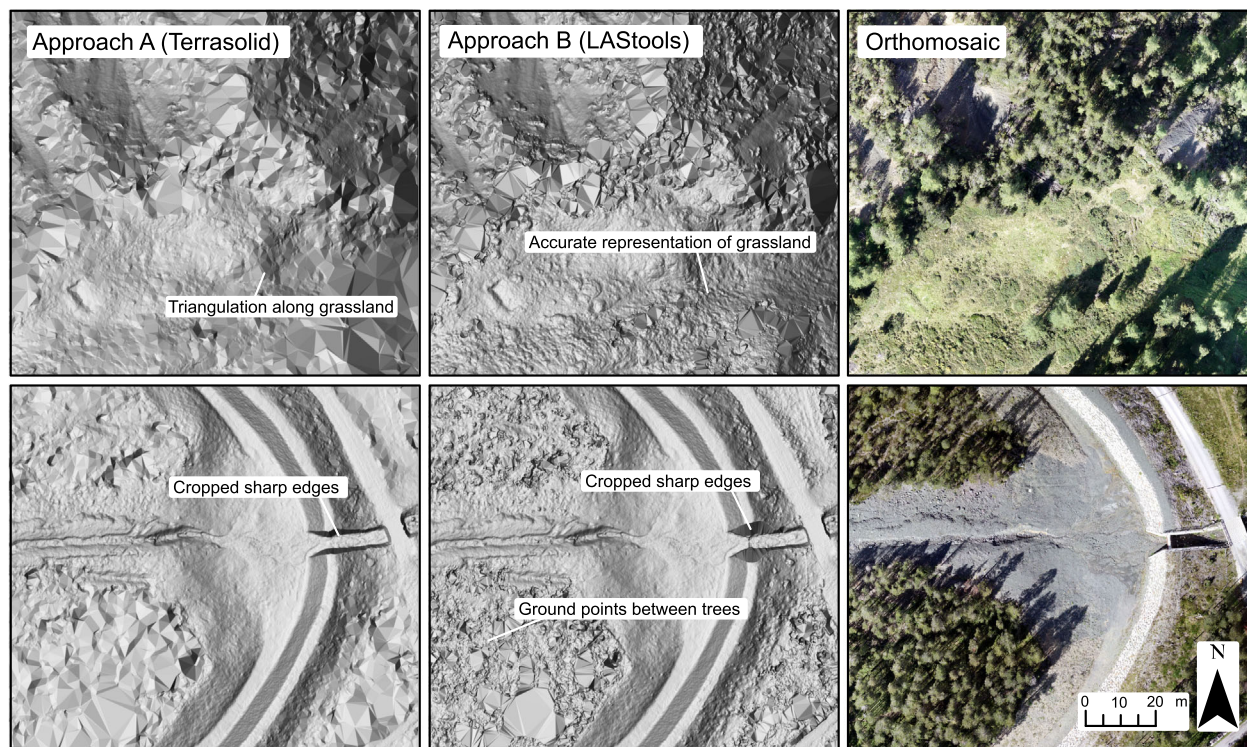


**FIGURE 7** Qualitative comparison of LAStools and Terrasolid. Low vegetation such as grass is often interpolated with the Terrasolid algorithm. Sharp edges from constructions are less well preserved with LAStools than Terrasolid [Color figure can be viewed at [wileyonlinelibrary.com](https://onlinelibrary.wiley.com/doi/10.1002/esp.5585)]

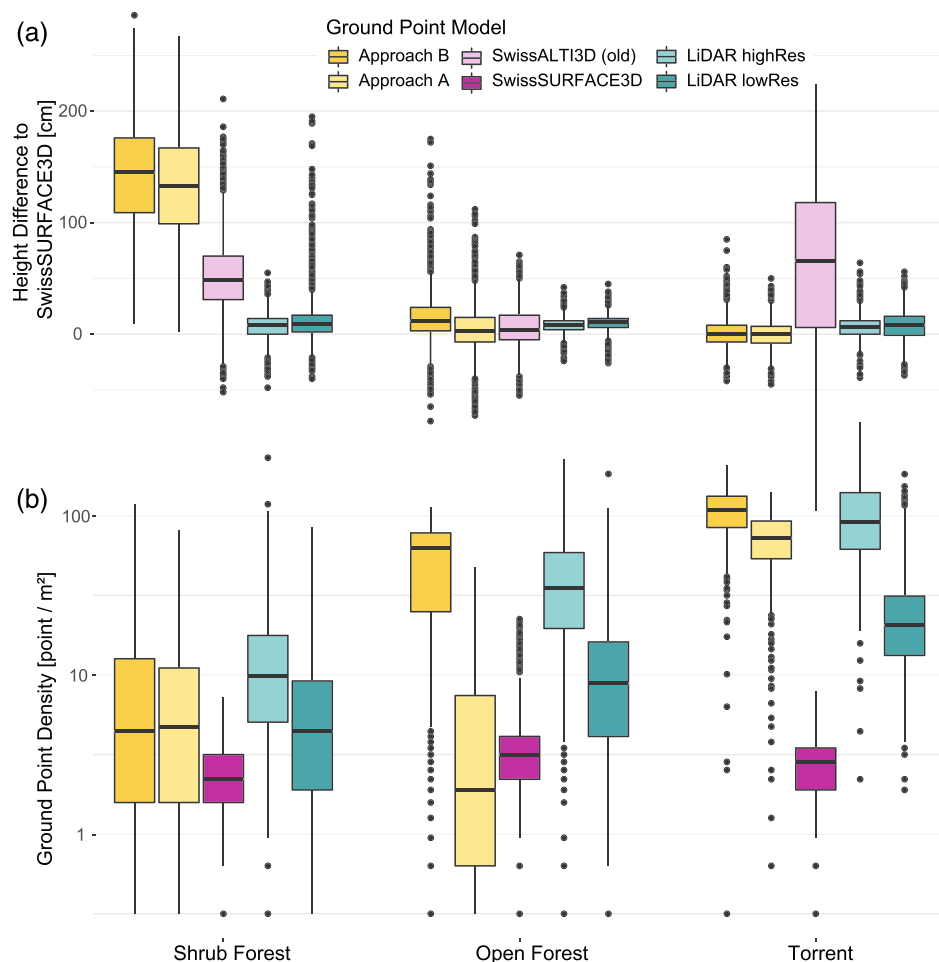


**FIGURE 8** Boxplots for three sample areas using 2000 random sample points (shrub forest, open forest and an area covering the torrent). The Terrasolid (Approach A) and LAStools (Approach B) routines are based on photogrammetric point data originating from a WingtraOne UAV flight. The LiDAR data (DJI M600 Pro with a Riegl miniVUX-3UAV) are classified with a standard LAStools routine. (a) Height deviation in comparison with the swissSURFACE3D data. (b) Ground point density of different ground point clouds [Color figure can be viewed at [wileyonlinelibrary.com](https://onlinelibrary.wiley.com/doi/10.1002/esp.5585)]

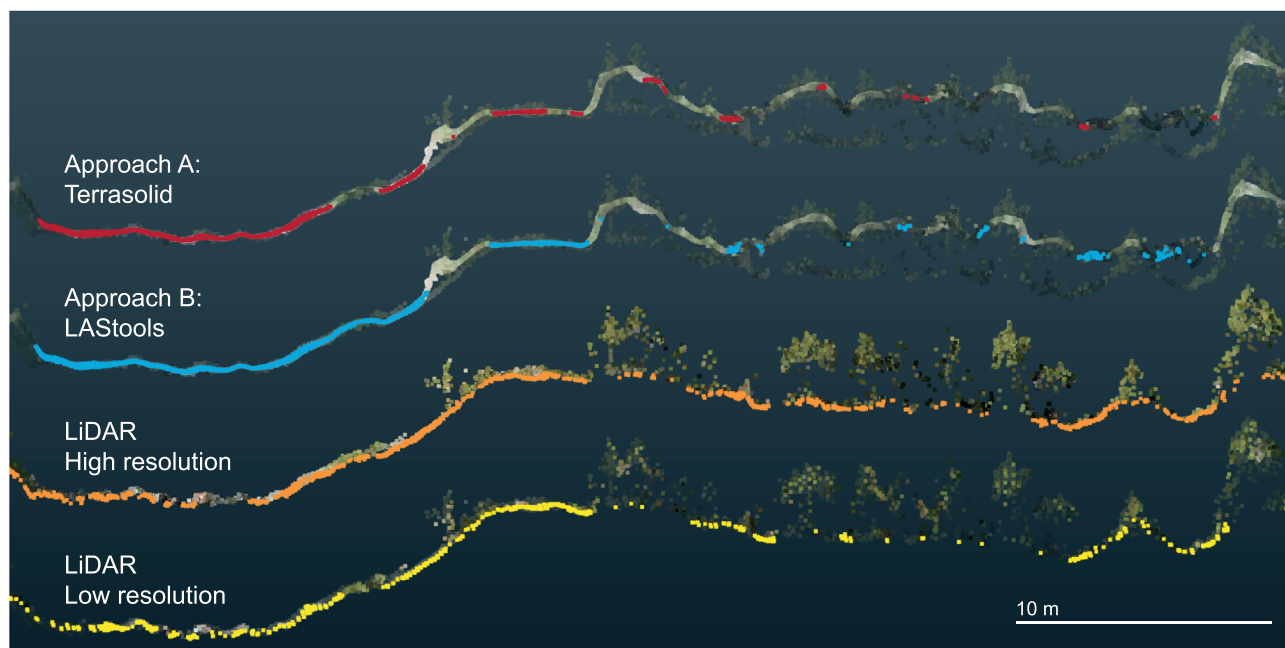


**FIGURE 9** Along densely vegetated shrub forests photogrammetric-derived routines are strongly limited, and classified ground points (colour highlighting) tend to be clearly above the LiDAR-based ground points. The ground point density of the high-resolution LiDAR along the densely vegetated areas is clearly superior compared to the low-resolution survey. For better comparison, all ground points are plotted with the unclassified high-resolution LiDAR point cloud in the background [Color figure can be viewed at [wileyonlinelibrary.com](https://onlinelibrary.wiley.com/doi/10.1002/esp.5585)]

torrent. In sparsely vegetated areas, the LiDAR ground point density between the high and low resolution shows the largest variances.

### 4.3 | Torrential properties

Geometry measures are calculated every 0.5 m. The derived statistical geometry estimates may be used within geomorphological assessment approaches such as SEDEX (Kienholz et al., 2010; Frick et al., 2011).

We tested automated extraction of the torrential properties within the catchment Arelen and Fraschmardin (see Figure 10). The automatic OBIA-based classification of the torrential extent with eCognition shows its limitations, especially within vegetated areas and/or steep adjacent slopes. Polygons representing the torrential extent were additionally manually digitized in ArcGIS (Esri, 2022) to quantify these uncertainties, and geometry attributes for each homogeneous section were estimated in the field (see Figure 1). Figure 11 contrasts field estimates with OBIA, GIS and field-based measures for Fraschmardin torrent bed width, torrent inclination and embankment height for the sections A–H as shown in Figure 1. The inclination of the torrent bed along the channel is declining with altitude, with a torrent bed width showing little change. The embankment width features strong variations, caused by local conditions such as residual boulders, trees and shrubs.

The average deviations between the field estimates and the extracted measures (median for each section) for the Fraschmardin catchment are about 22%, if focusing on the areas where the limitations of the approach can be neglected the error is reduced to approximately 12%. Obviously, for small geometrical extents, the field measurement accuracy weights in stronger on the relative error. The extraction of the torrential properties is limited along the uppermost catchment especially due to poorly delineated embankments as the

adjacent slopes are rising steeply (see Figure 1). More specifically, the inclination deviates 10% on average, the torrent width 14.5% and the embankment 11%. Nevertheless, such terrain is also challenging to assess in the field.

The torrent bed inclination (see Figure 10a/e) provides valuable information for dividing the catchment into homogeneous sections, the ability to provide locations within the channel where debris flows may initiate or where erosion is likely to occur. The high resolution of the automatically derived inclination allows for the characterization of specific elements such as check dams and local incisions. The torrent bed width is strongly influenced by large boulders and collapsed embankments. Derived values are highly consistent with field measurements.

Misclassified embankments have a direct influence on the derived cross-section area, which was derived from a trapezoidal area based on the average height of the two embankment heights and the width of the torrential extent. The two-sided average leads to more robust results. As we have compared the cross-section area derived from GIS and OBIA (see Figure 10c/d,g/h) we observed that the derived OBIA cross-section area is noisier, especially along densely vegetated terrain. The manually drawn torrential extent is not always fully correct, as it is based on only one subjective estimation. Further, figures and detailed boxplots featuring additional parameters of interest are found in Appendix C (Figures C1–C4).

## 5 | DISCUSSION

In the framework of this study, we have worked with different equipment and data sources with varying spatial resolutions and two different approaches for deriving surface data. UAV-based terrain data have a main advantage to be acquired on a large scale with a high temporal resolution (Walter et al., 2022) at relatively low costs and



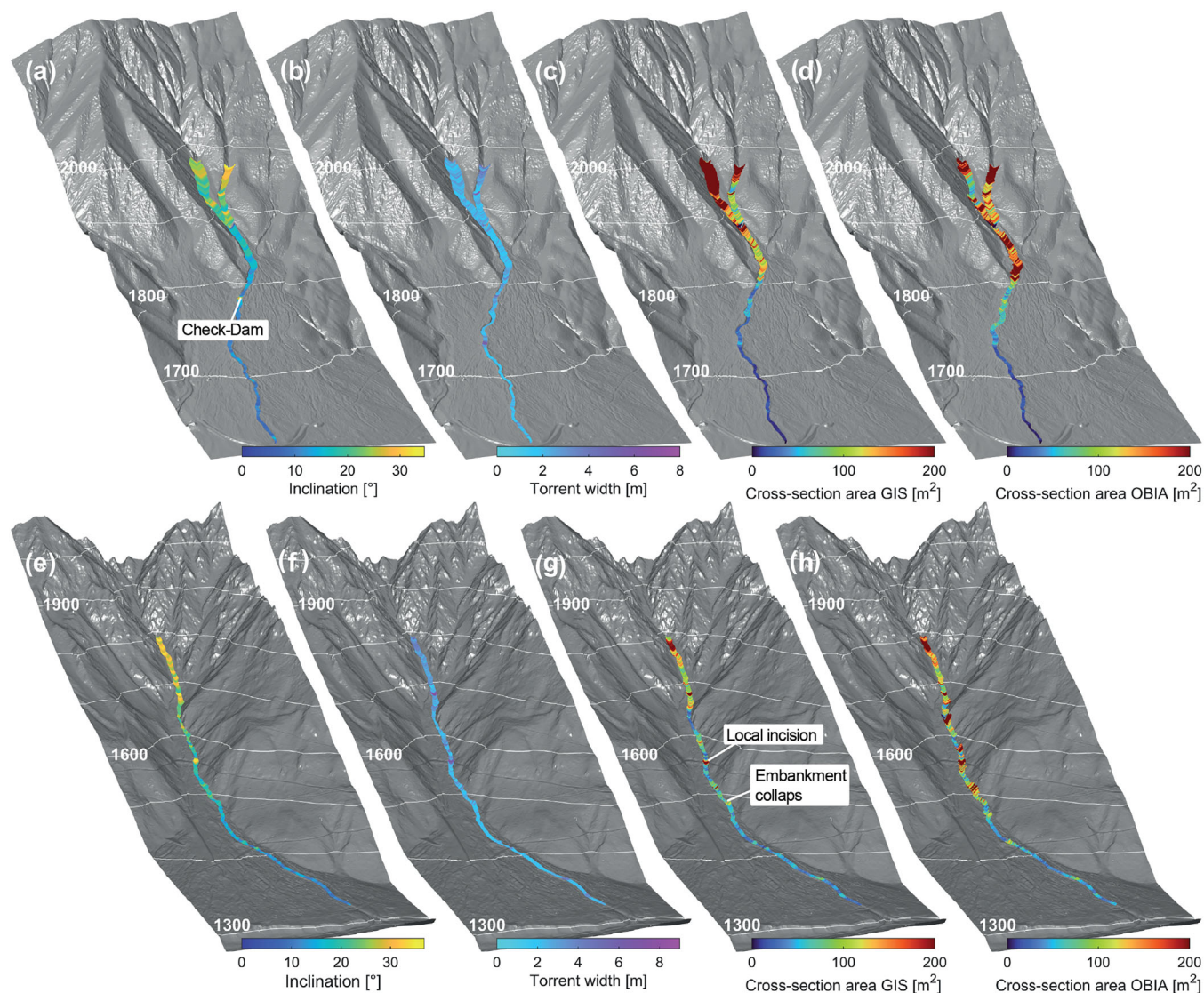


**FIGURE 10** Extracted torrential properties of (a–d) Arelen and (e–h) Fraschmardin: (a/e) inclination torrent bed, (b/f) Torrent bed width, (c/g) cross-section area based on manually drawn embankment polygon in GIS and (d/h) cross-section area based on automatic OBIA [Color figure can be viewed at [wileyonlinelibrary.com](https://onlinelibrary.wiley.com/doi/10.1002/esp.5585)]

limited risks (Giordan et al., 2018). We present the potential and the limitations of UAV-based torrent analysis, focusing on the parameters that were investigated and measured in the presented study and indicate the potential relevance for hazard assessment.

## 5.1 | Data acquisition and data quality

Data acquisition using photogrammetric UAVs in debris-flow-prone catchments is demanding for various reasons. The steep and complex terrain requires careful flight planning (Giordan et al., 2018). Large altitude differences need intensive power consumption. Large birds, such as eagles, can attack. If damaged, the systems are often not recoverable on a steep mountain slope. Flights for the acquisition of parameters in torrents need to be carried out in a time window without snow, with as few green leaves as possible, and sensitive wildlife should not be disturbed. Weather conditions such as strong winds must always be kept in mind.

The different data sources used provide varying spatial resolutions between 2 and 0.04 m. For the application of the extraction of

torrential properties, we found a resolution of 0.25 m to be sufficient. Areal wide data sources such as the swissALTI3D provide a 2 m resolution, which is too low for the application along typical alpine torrents. This product in particular suffers from a low temporal update frequency of 6 years and is equally the heritage of well-established, but not necessarily the currently best available technology. The swissALTI3D is produced based on airborne photogrammetry and low-resolution LiDAR flight missions. Photogrammetrical UAV flight missions produce high-resolution DTMs (below 0.1 m) in nonvegetated areas with a temporal resolution as desired for the application needs.

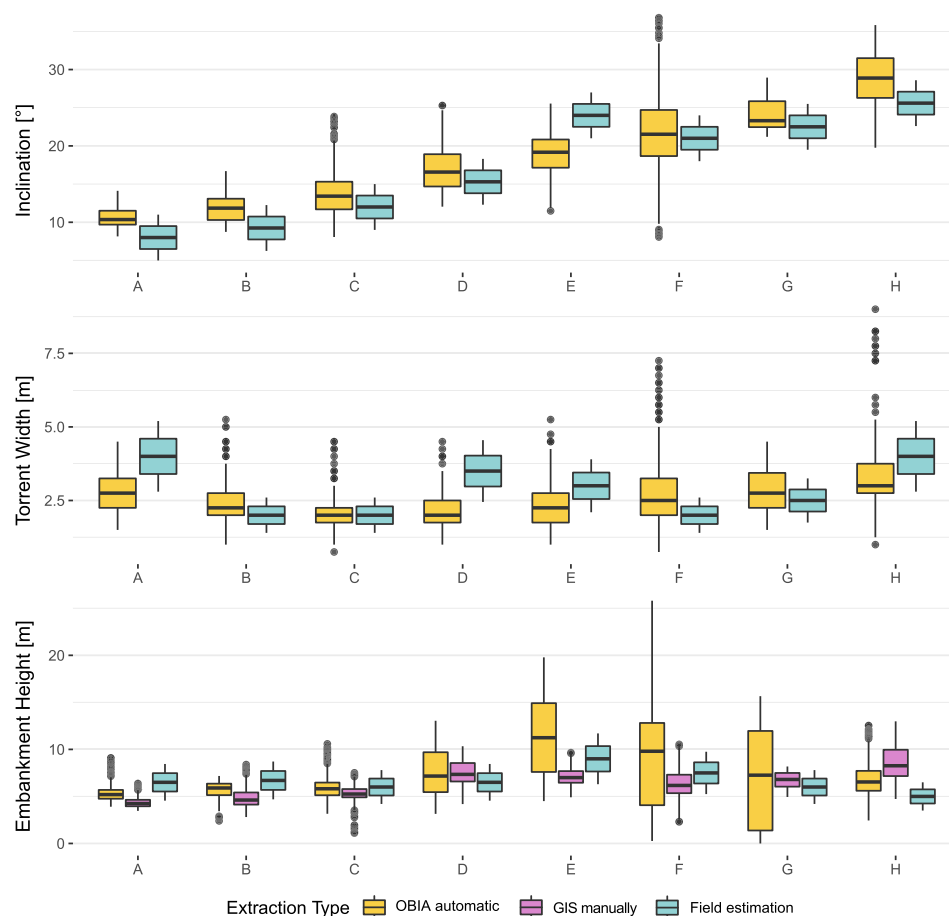
The observed xy-error is <0.04 m (see Table 3) and therefore in comparable range with other RTK-based SfM studies such as Nota et al. (2022), which show xy-errors <0.02 m. The slightly lower accuracy may be explained by steep topography. Our z-error is close to 0.06 m and even better than the data of Nota et al. (2022).

However, the discussed use case of torrential property identification does not require data accuracy higher than 0.25 m. Hence, systematic errors below this threshold can be neglected.

The WingtraOne is capable of flying over large areas, as it uses Tailsitter VTOL technology. A rather high flight altitude (~200 m)



**FIGURE 11** Comparison of the torrent parameters of the Franschmardin catchment. OBIA and manually extracted GIS values were displayed according to their distribution and field measurements with their survey uncertainties, respectively. Specific torrential sections (A–H) can be found in Figure 1. The inclination is derived over a distance of 10 m. Here, we show the orographic left embankment height. The resulting values of torrent bed width and inclination are consistent along the field- and GIS-based extraction. The OBIA-based embankment measurements show a particularly large variation along densely vegetated and landslide-prone areas [Color figure can be viewed at [wileyonlinelibrary.com](https://onlinelibrary.wiley.com)]



holds the advantage that the data acquisition time is efficient and the tilt effect of tall trees is of minor importance. Oblique pictures may hold the advantage along forested areas that there are not as many occlusion effects (Díaz et al., 2020). Further improvements may be achieved with the application of different flight altitudes and circular flight patterns (Roncoroni et al., 2022). However, for such flight settings, a quadcopter UAV is needed. Along heavily incised terrain, multirotor UAVs hold the further advantage of better manoeuvrability such as to hover, fly narrow turns and follow the terrain. However, these additional capabilities of multicopter systems are often outweighed by the main drawback of limited flight coverage due to shorter flight time.

## 5.2 | DTM generation based on photogrammetric UAV data

Point cloud data retrieved from photogrammetric UAVs need to be classified into ground and further points. Classification routines only based on either TIN densification or native filtering do not provide reliable results in alpine terrain, as they have difficulties distinguishing steep and rough hill slopes from shrub forests. The combination of RGB-based classification with other algorithms provides the most reliable results (Anders et al., 2019).

The Terrasolid-based Approach A aims to generate a smooth terrain surface and subsequently applies the classification algorithm on this smoothed surface. Due to the smoothing, the TIN densification becomes more robust. With the LAsTools algorithm (Approach B), the

goal to keep all potential ground points is pursued also below the uppermost vegetation layer. This noisy surface is rather challenging for the TIN densification algorithm. A second coarse TIN densification and various distance calculations were needed to remove the remaining noise. With this twofold routine, it was possible to preserve the highly dense photogrammetric surface. The noise removal may be further refined and improved. Especially the exertion of low noise removal as done in de Haas et al. (2020) could further improve Approach B. However, the application of multiple TIN densifications will remain an indispensable for the removal of vegetation along the whole torrential catchment. A further major drawback is experienced along highly active landslides, which make the difference calculation with the reference height model impossible. Approach A has the major advantage that it does not require a reference height model to differentiate between grass and high vegetation, but consequently, it is not very robust. In many regions of the world, meterscale DTMs, which are a prerequisite for Approach B, are these days not available area wide. While the specific parameter choices found in Appendix A would need confirmation and/or adjustment for different landcover/vegetation densities for both approaches, the fundamental advantage of Approach A is its instant applicability at any given region worldwide. Both elaborated approaches are based on various processing steps. This structure holds the advantage that the algorithm can be repeatedly adjusted, and parameters where needed can be optimized, but it implies sufficient understanding of the behaviour of such complex algorithms. Simple algorithms such as from Zhang et al. (2016) could be applied more easily, but as soon as the terrain becomes complex, the results are often not applicable. A next step could include

the validation of the accuracy of the presented approaches within triangulated areas with respect to the surface roughness, as it is known that this parameter has a significant impact on simulation results (Schraml et al. 2015).

### 5.3 | Torrent analysis

Here, we present the potential and the limitations of UAV-based torrent analysis, focusing on the parameters that were investigated and measured in the presented work, and point out their relevance for hazard assessment. A torrent analysis involves a qualitative and quantitative characterization of the catchment. Three important components—hydrology, sediment (type, size, distribution) and alluvial/dead wood—are typically assessed. The scope of any torrent analysis must be clearly defined in close cooperation with stakeholders. Important sources such as the event and protective structure cadastres are consulted. Hydrological calculations are used to estimate torrent runouts. For the assessment of deadwood, the respective forest area is important. With regard to sediments, the terrain and torrent bed are analysed. Possible torrent and slope processes, such as bed erosion and landslides, are identified using geodata often at a discrete point in time. Debris-flow hazard assessment requires a combination of fieldwork, numerical methods and expert knowledge. The clear communication of uncertainties and the reproducibility of the assessment is of great importance (Jakob, 2005). The availability of high-resolution and up-to-date DTMs is crucial for an accurate hazard assessment and especially for numerical modelling. The availability and reproducibility of detailed torrent parameters over a large area ultimately define the accuracy of the scenario development. UAV-based methods facilitate a more objective torrent assessment; nonetheless, fieldwork will remain indispensable and can be concentrated at specific critical locations in the torrent, eventually using computer-aided preselection of key sections and weak points based on drone-based measurements to put the hazard experts' valuable time and wits to its most efficient use. We have collected terrain surface data in two test areas to evaluate torrent parameters. UAV-based products offer the possibility of a fast, reliable and objective assessment of the catchment. The raw, dense point cloud provides a three-dimensional representation of the catchment. With small UAVs, steep, inaccessible terrain can be investigated. Active torrential areas could be targeted with repetitive flight missions yielding detailed time series information about torrent evolution (de Haas et al., 2022). Sediment transport patterns provide an indication of the expected frequency of future events and reconstructions of debris-flow events can help to improve numerical models and calibrate parameters for site-specific numerical simulations for the subsequent runout analysis.

The inclination of the torrent bed can provide a rough estimate of the potential erosive power of a debris flow (Rickenmann, 2014). Steep inclinations are associated with higher debris-flow velocities and therefore higher basal shear stresses. These higher shear stresses can be compared with the material properties of the torrent bed to assess erosion. The fundamental challenge to accurately estimate erosion rates is an accurate quantification of the bed material properties (Berger et al., 2011; Iverson et al. 2011). For this, the grain size distribution may provide an indication of sediment availability and erosion rates. Methods that derive this information from topography seem to

provide the most consistent results (e.g., Heritage & Milan, 2009; Schneider et al., 2015). However, more quantitative studies along debris-flow-prone catchments are needed for a more detailed understanding.

The torrent bed width is strongly influenced by large boulders and collapsed embankments. It shows good consistency along the field- and GIS-based extraction. The exact determination of torrent bed width remains very challenging. On the one hand, this is due to constant small-scale changes and, on the other hand, due to the transition from the channel bed to the channel slope cannot always be clearly determined. This difficulty exists not only in UAV-derived determination, but also in field analysis. The embankment height depends on various factors, such as incision, landslide activity in the channel slope, vegetation cover, etc.. The automatically derived measurements show a general consistency with field- and GIS-based extraction. Again local conditions such as residual boulders, trees and shrubs play a crucial role. The two-sided cross-section classification we applied is fairly robust, and the encountered limitations relate to the estimated capacity deviating from reality due to the simplified trapezoidal cross-section computation.

Attempts to estimate a debris-flow volume based on empirical relationships show a wide solution range and therefore limitations for site-specific hazard assessment (Rickenmann, 1999). Fieldwork is therefore important to specify parameters relevant to debris-flow volume analysis. Delineation of the embankment is important to assess the areas delivering sediment to the torrent. The accurate delineation of the embankment is highly complex and challenging in the field as well automatically based on UAV data. Especially, when the neighbouring slope features a similar inclination as the embankment. We found that the derived median geometry measures along the torrent segments show strong agreement with field surveys. This suggests that repeated surveys with sufficient accuracy provide an promising tool for the assessment of the expected debris-flow volume. The question of how much material will be eroded remains, however, a highly difficult question and is strongly dependent on event type and progression (Berger et al., 2011; Iverson et al., 2011). The contributing volume, derived from erosive capacity and contributing area, can be understood as the potential erosion volume.

The presented automated quantification of torrent characteristics facilitates efficient planning of fieldwork. Key parameters such as the cross-section area and slope identify homogeneous sections, which can be further used with geomorphologic assessment methods (e.g., Frick et al., 2008, 2011). The expected debris-flow erosion rates may be assessed more objectively with the support of UAV data. A sound quantification of volumes originating from hillslopes processes and the consideration of further factors such as jamming, condition of protective structures and old traces remain to be derived in large part from field surveys. The combination of field observations, experience and expert knowledge is key for comprehensive hazard assessment. The information gain driven by an available time series of a changing torrent is potentially substantial. The smaller the uncertainties in the torrent analysis, the more accurate the scenario definition and runout analysis and consequently the hazard map.

To conclude, we summarize the advantages and the disadvantages that are associated with UAV-based torrent assessment in Table 4.

**TABLE 4** Summary of advantages and disadvantages of UAV-based assessment of torrents.

	Pro	Contra
Costs	Cheaper than helicopter inspections	High set-up costs (software, computer, UAV, training)
Time demand	Fieldwork can be addressed more specifically	Additional workload (UAV flight 2–3 h; processing 1 h)
Planning	Can be combined with field work	Stable weather, no snow, little leaves as possible
Reproducibility	Clear data basis available	Some classification algorithms need to be applied
Approach A	No need of reference height model	Erroneous classification of grassland and surface smoothing
Approach B	Accurate on rough surfaces and grassland	Need of accurate coarse reference height model
LiDAR UAV	Produces accurate DTM in dense vegetation	High equipment costs (~100 000 CHF), only small areas
VTOL photogrammetric UAV	Captures large areas	High equipment costs (~35 000 CHF), limited by vegetation
Torrent analysis	Overview, objective segmentation of sections	Limited to clearly defined torrent beds
Runout analysis	Less field measurements are needed	Limited near bridge curvatures and dikes
Erosion	Contributing area can be derived automatically	Depth is not possible to derive automatically
Change quantification	Sophisticated distance measure with M3C2	Limited by occlusion due to vegetation

## 6 | CONCLUSIONS AND OUTLOOK

In this work, we present two workflows to classify photogrammetric-derived point clouds in alpine terrain. Further, we introduce an approach for automated acquisition and parametrization of debris-flow-prone torrent channel properties. This represents important progress because it provides area-wide information on the condition and nature of the surface in and around the channel. In addition, repeated measurements would provide a better understanding of the processes and developments, which in turn allows better interpretation and forecasting of what is happening in the channel. The presented methodology yields continuous geometry data along the torrent, which is a major advantage compared to point-based field surveys or related to individual channel sections. Cross-validation of our UAV-derived data sets with independent field measurements shows a strong agreement. The inclination in the Fraschmardin catchment for example deviates on average by 10%, the torrent width by 14.5% and the embankment by 11% in well-performing sections. Large discrepancies of over 100% are found along sections, where retrospectively a poor field estimation was obtained, or where automatic extraction was limited by steep adjacent slopes and/or dense vegetation patterns. However, we assume that the roughly estimated field measurements are often less accurate than the automatically extracted data. Traceability and reproducibility is often experienced insufficient with field methods. This is partly due to insufficient documentation and unfortunately often lack of available time. Carefully documented and accurately measured fieldwork may lead to accurate results; however, they stay labour intensive and remain only point measures. A large-scale independent study with accurate independent field measurements would need to be conducted by practitioners to prove the reliability of these findings. Issues with dense vegetation along the embankment could be solved by applying the algorithm to LiDAR UAV-based terrain data with very high point densities (>200 points/m<sup>2</sup>). Difficulties caused by steep adjacent slopes will remain. At the current stage, the costs for LiDAR-based surveys are a multiple higher than photogrammetrical surveys. We, therefore, propose to acquire the data photogrammetrically and process the data with the proposed classification routines. Along densely vegetated areas of the catchment, additional LiDAR flights can be conducted to further improve the results. In the future, we

expect that the costs for high-quality, drone-based LiDAR sensors will decrease substantially, enabling the acquisition of accurate DTM data even in densely vegetated areas.

Once a large database of many different torrents with UAV and manual measurements is available, the developed extraction algorithms could be coupled with machine learning approaches. Fieldwork will always remain a mandatory input in the assessment process. At the present stage, the available sediment, the erosion capacity, the slope processes and the condition of the structures can only be properly assessed on the basis of accurate fieldwork. In conclusion, a sound hazard assessment remains challenging. Further interdisciplinary research that couples remote sensing techniques and hazard assessment procedures for a wider variety of study sites are indispensable.

### AUTHOR CONTRIBUTIONS

Gregor Schmucki wrote the paper and performed the entire data analysis; Yves Bühler, Andreas Stoffel and Mauro Marty supported all the remote sensing measurements and data analysis; Perry Bartelt and Ch. Graf contributed to debris flow mechanics and field visits; Christoph Huggel and Andrin Caviezel supported the data analysis, computer infrastructure and paper formulation and editing.

### ACKNOWLEDGEMENTS

This work was performed within the framework of the WSL research programme CCAMM, Task 2: Dynamics. It was directly financed by CCAMM and the RAMMS research teams. We thank the WSL for the financial support of this project. Open access funding provided by ETH-Bereich Forschungsanstalten.

### ENVIDAT DATA AVAILABILITY

Schmucki, G. (2023). Photogrammetric Drone Data and derived Ground Classification Wolfgang Arelen. EnviDat. <https://www.doi.org/10.16904/envidat.391>

### DATA AVAILABILITY STATEMENT

Data such as processed dense point cloud, classified ground point clouds and resulting digital terrain models of the Arelen catchment will be made available in a persistent ENVIDAT data repository upon publication (<https://www.doi.org/10.16904/envidat.391>).



## ORCID

Gregor Schmucki  <https://orcid.org/0000-0003-1875-5885>

## REFERENCES

- AGNES. (2022) AGNES—Automated GNSS Network for Switzerland. Available from: <https://pnac.swisstopo.admin.ch/pages/en/agnes.html>
- Abele, G. (1974) Bergstürze in den Alpen: ihre Verbreitung, Morphologie und Folgeerscheinungen, Bände 23–25 Bergstürze in den Alpen: ihre Verbreitung, Morphologie und Folgeerscheinungen, Gerhard Abele Ausgabe 25 von Wissenschaftliche Alpenvereinshefte, Deutscher Alpenverein, ISSN 0084-0912. Wissenschaftliche Alpenvereinshefte: München.
- Adams, M., Fromm, R. & Lechner, V. (2016) High-resolution debris flow volume mapping with unmanned aerial systems (UAS) and photogrammetric techniques. *The International Archives of the Photogrammetry, Remote Sensing and Spatial Information Sciences*, 41, 749–755.
- Anders, N., Valente, J., Masselink, R. & Keesstra, S. (2019) Comparing filtering techniques for removing vegetation from UAV-based photogrammetric point clouds. *Drones*, 3(3), 61. Available from: <https://www.mdpi.com/2504-446X/3/3/61>
- BAFU. (1997) Berücksichtigung der Hochwassergefahren bei raumwirksamen Tätigkeiten. Bundesamt für Umwelt (BAFU). Available from: <https://www.bafu.admin.ch/bafu/de/home/themen/thema-naturgefahren/naturgefahren--publikationen/publikationen-naturgefahren/beruecksichtigung-der-hochwassergefahren-bei-raumwirksamen-taeti.html>
- BAFU. (2019) Naturereigniskataster stürme. Available from: <https://feds.eiam.admin.ch/adfs/l/>
- Berger, C., McArdell, B.W. & Schlunegger, F. (2011) Sediment transfer patterns at the Illgraben catchment, Switzerland: implications for the time scales of debris flow activities. *Geomorphology*, 125(3), 421–432. Available from: <http://www.sciencedirect.com/science/article/pii/S0169555X10004484>
- Bühler, Y., Adams, M.S., Bösch, R. & Stoffel, A. (2016) Mapping snow depth in alpine terrain with unmanned aerial systems (UASs): potential and limitations. *The Cryosphere*, 10(3), 1075–1088. Available from: <https://tc.copernicus.org/articles/10/1075/2016/>
- Cucchiari, S., Cavalli, M., Vericat, D., Crema, S., Llana, M., Beinat, A., Marchi, L. & Cazorzi, F. (2018) Monitoring topographic changes through 4D-structure-from-motion photogrammetry: application to a debris-flow channel. *Environmental Earth Sciences*, 77(18), 632. Available from: <https://doi.org/10.1007/s12665-018-7817-4>
- de Haas, T., Kruijt, A. & Densmore, A.L. (2018) Effects of debris-flow magnitude-frequency distribution on avulsions and fan development. *Earth Surface Processes and Landforms*, 43(13), 2779–2793. Available from: <https://onlinelibrary.wiley.com/doi/abs/10.1002/esp.4432>
- de Haas, T., McArdell, B.W., Nijland, W., Åberg, A.S., Hirschberg, J. & Huguenin, P. (2022) Flow and bed conditions jointly control debris-flow erosion and bulking. *Geophysical Research Letters*, 49(10), e2021GL097611. Available from: <https://agupubs.onlinelibrary.wiley.com/doi/abs/10.1029/2021GL097611>
- de Haas, T., Nijland, W., de Jong, S.M. & McArdell, B.W. (2020) How memory effects, check dams, and channel geometry control erosion and deposition by debris flows. *Scientific Reports*, 10(1), 14024. Available from: <https://www.nature.com/articles/s41598-020-71016-8>
- Díaz, G.M., Mohr-Bell, D., Garrett, M., Muñoz, L. & Lencinas, J.D. (2020) Customizing unmanned aircraft systems to reduce forest inventory costs: can oblique images substantially improve the 3D reconstruction of the canopy? *International Journal of Remote Sensing*, 41(9), 3480–3510. Available from: <https://doi.org/10.1080/01431161.2019.1706200>
- Ducard, G. J. J. & Allenspach, M. (2021) Review of designs and flight control techniques of hybrid and convertible VTOL UAVs. *Aerospace Science and Technology*, 118, 107035. Available from: <https://www.sciencedirect.com/science/article/pii/S1270963821005459>
- Esri. (2022) ArcGIS Pro geoprocessing tool reference. California: ESRI Inc.. Available from: <https://pro.arcgis.com/en/pro-app/latest/tool-reference/main/arcgis-pro-tool-reference.htm>
- Frick, E., Kienholz, H. & Romang, H. (2011) *Sedex Anwenderhandbuch*. Geographisches Institut der Universität Bern: Bern.
- Frick, E., Kienholz, H. & Roth, H. (2008) Sedex—eine praxistaugliche Methodik zur Beurteilung der Feststofflieferung in Wildbächen. Sedex—a practical tool to estimate sediment deliveries in mountain torrents, INTERPRAEVENT 2008—Conference Proceedings, vol. 1. Dornbirn: Interpraevent.
- Giordan, D., Hayakawa, Y., Nex, F., Remondino, F. & Tarolli, P. (2018) Review article: The use of remotely piloted aircraft systems (RPASs) for natural hazards monitoring and management. *Natural Hazards and Earth System Sciences*, 18(4), 1079–1096. Available from: <https://nhess.copernicus.org/articles/18/1079/2018/nhess-18-1079-2018.html>
- Graf, C., Christen, M., McArdell, B.W. & Bartelt, P. (2019) An overview of a decade of applied debris-flow runout modeling in Switzerland: challenges and recommendations. In: Kean, J.W., Coe, J.A., Santi, P.M. & Guillen, B.K. (Eds.), *Association of environmental and engineering geologists special publication: Vol. 28. Debris-flow hazards mitigation: mechanics, monitoring, modeling, and assessment*. Association of Environmental and Engineering Geologists, Colorado USA: DFHM7, pp. 685–692.
- Heritage, G.L. & Milan, D.J. (2009) Terrestrial Laser Scanning of grain roughness in a gravel-bed river. *Geomorphology*, 113(1), 4–11. Available from: <https://www.sciencedirect.com/science/article/pii/S0169555X09001482>
- Hungr, O., Evans, S.G., Bovis, M.J. & Hutchinson, J.N. (2001) A review of the classification of landslides of the flow type. *Environmental and Engineering Geoscience*, 7(3), 221–238. Available from: <https://pubs.geoscienceworld.org/aeg/eeg/article-abstract/7/3/221/60609/A-review-of-the-classification-of-landslides-of>
- Hürlimann, M., Coviello, V., Bel, C., Guo, X., Berti, M., Graf, C. et al. (2019) Debris-flow monitoring and warning: review and examples. *Earth-Science Reviews*, 199, 102981. Available from: <http://www.sciencedirect.com/science/article/pii/S0012825219302764>
- Iverson, R.M. (1997) The physics of debris flows. *Reviews of Geophysics*, 35(3), 245–296. Available from: <https://agupubs.onlinelibrary.wiley.com/doi/abs/10.1029/97RG00426>
- Iverson, R.M., Reid, M.E., Logan, M., LaHusen, R.G., Godt, J.W. & Griswold, J.P. (2011) Positive feedback and momentum growth during debris-flow entrainment of wet bed sediment. *Nature Geoscience*, 4(2), 116–121.
- Jakob, M. (2005) Debris-flow hazards and related phenomena. In *Debris-flow hazard analysis*. Berlin, Heidelberg: Springer, pp. 411–443. Available from: <https://doi.org/10.1007/b138657>
- Jakob, M. (2021) Debris-flow hazard assessment: a practitioner's view. *Environmental & Engineering Geoscience*, 27(2), 153–166.
- Jakob, M. & Hungr, O. (2005) *Debris-flow hazards and related phenomena*. Berlin, Heidelberg: Springer.
- Kienholz, H., Frick, E. & Gertsch, E. (2010) Assessment tools for mountain torrents: SEDEX and bed load assessment matrix, International Symposium in Pacific Rim. Taipei, Taiwan: International research society Interpraevent.
- Koenderink, J.J., van Doorn, A. J. (1991) Affine structure from motion. *Journal of the Optical Society of America*, 8(2), 377–385. Available from: <http://www.osapublishing.org/josaa/abstract.cfm?URI=josaa-8-2-377>
- LASTools. (2022) *Efficient LiDAR Processing Software*. Gilching, DE: rapidlasso GmbH. Available from: <http://rapidlasso.com/LASTools>
- Maisch, M. (1981) Glazialmorphologische und gletschergeschichtliche Untersuchungen im Gebiet zwischen Landwasser- und Albulatal (Kt. Graubünden, Schweiz). Ph.D. Thesis, University Zurich.
- Melton, M.A. (1965) The geomorphic and paleoclimatic significance of alluvial deposits in Southern Arizona. *The Journal of Geology*, 73(1), 1–38. Available from: <https://www.jstor.org/stable/30066379>
- Niculita, M., Mărgărit, M.C. & Tarolli, P. (2020) Chapter 10 - Using UAV and LiDAR data for gully geomorphic changes monitoring. In: Tarolli, P. & Mudd, S.M. (Eds) *Developments in earth surface processes*, vol. 23. Elsevier, pp. 271–315. Available from: <https://doi.org/10.1016/B978-0-444-64177-9.00010-2>
- Nota, E.W., Nijland, W., de Haas, T. (2022) Improving UAV-SFM time-series accuracy by co-alignment and contributions of ground control

- or RTK positioning. *International Journal of Applied Earth Observation and Geoinformation*, 109, 102772. Available from: <https://www.sciencedirect.com/science/article/pii/S0303243422000988>
- Passalacqua, P., Belmont, P., Staley, D.M., Simley, J.D., Arrowsmith, J.R., Bode, C.A. et al. (2015) Analyzing high resolution topography for advancing the understanding of mass and energy transfer through landscapes: a review. *Earth-Science Reviews*, 148, 174–193. Available from: <http://www.sciencedirect.com/science/article/pii/S0012825215300015>
- Rickenmann, D. (1999) Empirical relationships for debris flows. *Natural Hazards*, 19(1), 47–77. Available from: <https://doi.org/10.1023/A:1008064220727>
- Rickenmann, D. (2014) *Methoden zur quantitativen beurteilung von gerinneprozessen in wildbächen*, vol. 9. Birmensdorf: Eig. Forschungsanstalt für Wald, Schnee und Landschaft WSL.
- Rickenmann, D. (2016) Debris-flow hazard assessment and methods applied in engineering practice. *International Journal of Erosion Control Engineering*, 9(3), 80–90.
- Roncoroni, M., Mancini, D., Kohler, T.J., Miesen, F., Gianini, M., Battin, T. J. & Lane, S.N. (2022) Centimeter-scale mapping of phototrophic biofilms in glacial forefields using visible band ratios and UAV imagery. *International Journal of Remote Sensing and Remote Sensing Letters*, 43(13), 4723–4757.
- Schmucki, G.R. (2022) Photogrammetrical UAV-based investigation of torrents. Master's Thesis, University of Zurich.
- Schneider, J.M., Rickenmann, D., Turowski, J.M. & Kirchner, J.W. (2015) Self-adjustment of stream bed roughness and flow velocity in a steep mountain channel. *Water Resources Research*, 51(10), 7838–7859. Available from: <https://onlinelibrary.wiley.com/doi/abs/10.1002/2015WR016934>
- Schraml, K., Oismüller, M., Stoffel, M., Hübl, J. & Kaitna, R. (2015) Debris-flow activity in five adjacent gullies in a limestone mountain range. *Geochronometria* 42(1). Available from: <https://content.sciendo.com/view/journals/geochr/42/1/article-geochr-2015-0007.xml.xml>
- Signer, A., Maggetti, M., Keller, F., Winkler, W., Weissert, H.J. & Pfiffner, O.A. (2018) Blatt 1197 Davos.—Geologischer Atlas Schweiz 1: 25 000, Erläuterungen 156.
- Swisstopo. (2022a) *Swissalti3d, das hochpräzise digitale höhenmodell der schweiz*. Bern, CH: Bundesamt für Landestopografie swisstopo. Available from: <https://www.swisstopo.admin.ch/de/geodata/height/alti3d.html>
- Swisstopo. (2022b) *Swissurface3d, das digitale oberflächenmodell der schweiz*. Bern, CH: Bundesamt für Landestopografie swisstopo. Available from: <https://www.swisstopo.admin.ch/de/geodata/height/surface3d-raster.html>
- Takahashi, T. (2007) *Debris flow: mechanics, prediction and countermeasures*. Taylor & Francis: London.
- Terrasolid. (2021) *Terrascan user guide*. Espoo, Finland: Terrasolid Ltd. Available from: <https://terrasolid.com/guides/tscan.pdf>
- Trimble. (2022) User Guide eCognition Developer. Trimble Geospatial. Available from: <https://docs.ecognition.com>
- Verhoeven, G. (2011) Taking computer vision aloft—archaeological three-dimensional reconstructions from aerial photographs with photostan. *Archaeological Prospection*, 18(1), 67–73. Available from: <https://onlinelibrary.wiley.com/doi/abs/10.1002/arp.399>
- Walter, F., Hodel, E., Mannerfelt, E.S., Cook, K., Dietze, M., Estermann, L. et al. (2022) Brief communication: An autonomous uav for catchment-wide monitoring of a debris flow torrent. *Natural Hazards and Earth System Sciences*, 22(12), 4011–4018. Available from: <https://nhess.copernicus.org/articles/22/4011/2022/>
- Westoby, M.J., Brasington, J., Glasser, N.F., Hambrey, M.J. & Reynolds, J. M. (2012) 'Structure-from-Motion' photogrammetry: a low-cost, effective tool for geoscience applications. *Geomorphology*, 179, 300–314. Available from: <http://www.sciencedirect.com/science/article/pii/S0169555X12004217>
- Wingtra (2022) WingtraOne—GEN II—technical specifications. Available from: <https://wingtra.com/wp-content/uploads/Wingtra-Technical-Specifications.pdf>
- Zhang, H., Aldana-Jague, E., Clapuyt, F., Wilken, F., Vanacker, V. & Van Oost, K. (2019) Evaluating the potential of post-processing kinematic (PPK) georeferencing for UAV-based structure- from-motion (SfM) photogrammetry and surface change detection. *Earth Surface Dynamics*, 7(3), 807–827. Available from: <https://esurf.copernicus.org/articles/7/807/2019/>
- Zhang, W., Qi, J., Wan, P., Wang, H., Xie, D., Wang, X. & Yan, G. (2016) An easy-to-use airborne LiDAR data filtering method based on cloth simulation. *Remote Sensing*, 8(6), 501. Available from: <https://www.mdpi.com/2072-4292/8/6/501>
- Zubrycky, S., Mitchell, A., McDougall, S., Strouth, A., Clague, J.J. & Menounos, B. (2021) Exploring new methods to analyse spatial impact distributions on debris-flow fans using data from south-western British Columbia. *Earth Surface Processes and Landforms*, 46(12), 2395–2413. Available from: <https://doi.org/10.1002/esp.5184>

**How to cite this article:** Schmucki, G., Bartelt, P., Bühler, Y., Caviezel, A., Graf, C., Marty, M. et al. (2023) Towards an automated acquisition and parametrization of debris-flow prone torrent channel properties based on photogrammetric-derived uncrewed aerial vehicle data. *Earth Surface Processes and Landforms*, 48(9), 1742–1764. Available from: <https://doi.org/10.1002/esp.5585>



## APPENDIX A: GROUND CLASSIFICATION COMMANDS

## A. 1: LAStools commands

```

1 lasindex -i {}
2 lastile -i {} -tile_size 50 -buffer 5 -flag_as_withheld
3 las2las64 -i {} -copy_G_into_register -0 -scale_register 0 2.0 -copy_R_into_register
4   -subtract_registers 0 1 0 -copy_B_into_register 1
5   -subtract_registers 0 1 0 -copy_register_into_intensity 0
6 las2las64 -i {} -set_classification 0 -classify_intensity_above_as {} 3
7   -classify_intensity_below_as {} 2
8 las2las -i {} -keep_attribute_above 0 {} #color classification
9 lasheight64 -i {} -store_as_extra_bytes -ground_points {}
10 las2las64 -i {} -keep_class 3 -drop_attribute_above {} {} #height classification
11 las2las64 -i {} -set_classification 2 # green points near ground
12 lasmerge64 -i {} {} #merge classified height and green points near ground
13 lasduplicate64 -i {} #delete duplicate points
14 las2las -i {} -keep_class 2
15 las2las64 -i {} -set_classification 1
16 lasground_new64 -i {} -step 1 #1st ground classification
17 lasthin64 -i {} -step 1 -lowest -keep_class 2
18 lasground_new64 -i {} -step 6 #2nd ground classification
19 las2las64 -i {} -keep_class 2
20 lasnoise -i {} -step 1 -isolated 2 -remove_noise
21 lasheight -i {} -ground_points {} -do_not_store_in_user_data -keep_below 6
22 lasmerge64 -i {} -drop_withheld
23 lasheight -i {} -ground_points {} -do_not_store_in_user_data -classify_above 1 7 #diff 1st + 2nd gc
24 lasthin64 -i {} -odix_thin -olaz -keep_class 2 -step 0.1
25 lasmerge64 -i {} -drop_withheld #merge tiles
26 blast2dem -i {} -elevation -step 0.1 -merged -drop_withheld #DTM
27 blast2dem -i {} -hillshade -step 0.1 -merged -drop_withheld #hillshade

```

## A. 2: Terrasolid commands

```

1 FnScanClassifyClass("Any",1,0)
2 FnScanSort(12)
3 FnScanCutLowRel("Any",1,10,10,0.500,40)
4 FnScanClassifyLow(1,7,15,0.40,2.00,0)
5 FnScanClassifyIsolated("1",7,15,"1",3.00,0)
6
7 FnScanDeleteCass(7,0)
8 FnScanDeleteCass(10,0)
9 FnScanClassifySurface("1",8,0.050,1,0)
10 FnScanSmoothenYyz("8",0.200,"",0,0)
11 FnScanThinPoints("8",9,2,0,0.070,0.070,0)
12 FnScanClassifyLow(9,7,10,0.40,1.50,0)
13 FnScanClassifyIsolated("9",7,15,"8",2.00,0)
14
15 FnScanDeleteCass(1,0)
16 FnScanDeleteCass(7,0)
17 FnScanDeleteCass(8,0)
18 FnScanDistVbdvi("9",0.050)
19 FnScanSmoothenDist("9","",0.150,10,0)
20 FnScanClassifyDistance("9",17,0.000,9999.000,0)
21 FnScanClassifyGround("9",2,"2",1,60.0,75.00,15.00,1.00,1,8.0,0,2.0,0,0)

```

## APPENDIX B: PARAMETERS USED IN eCOGNITION

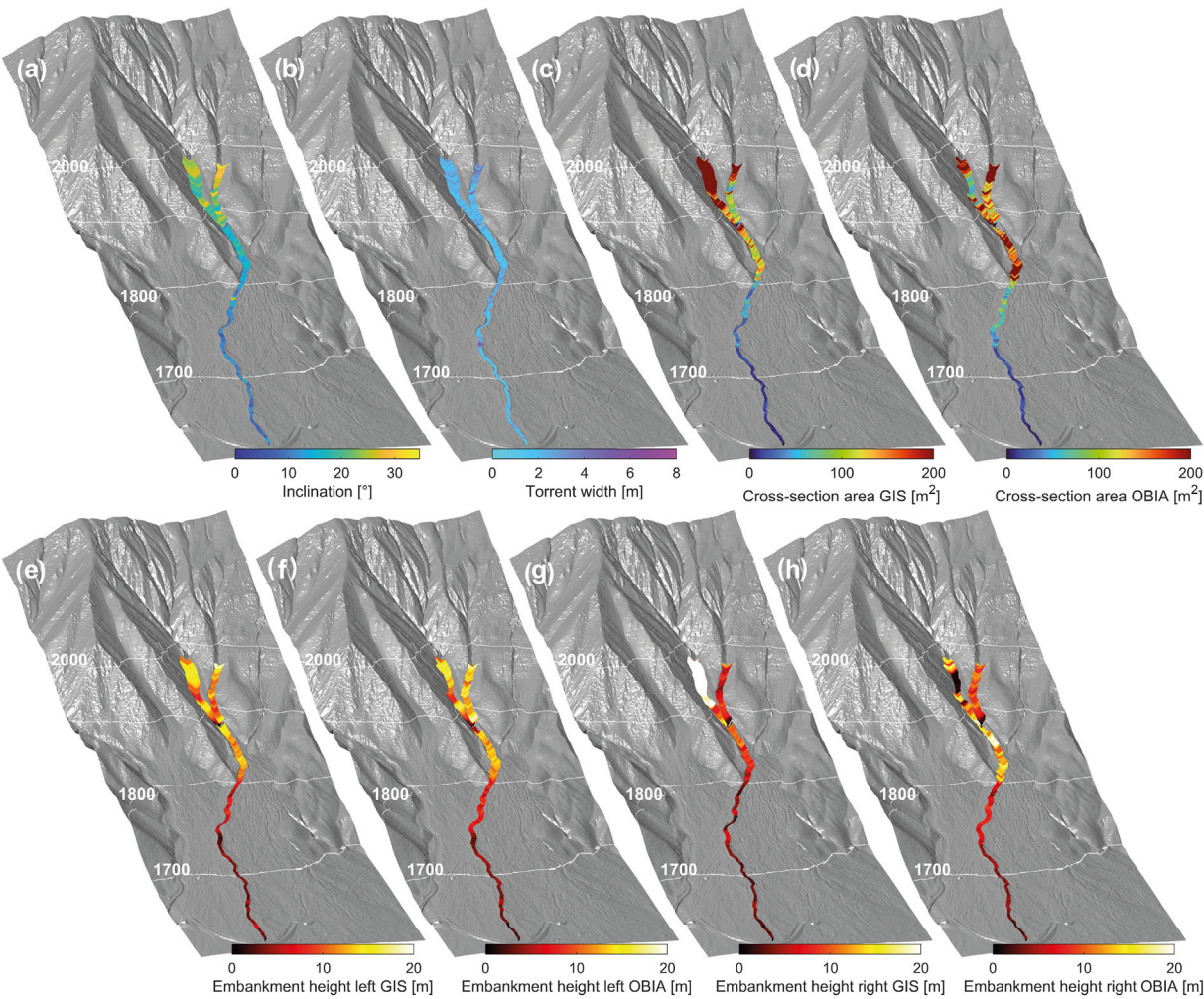
TABLE B1 Parameters used for the multiresolution segmentation within eCognition.

Entity	Weight
Slope	15
Distance map	4
Aspect n1	2
Aspect n2	2
Scale	80
Shape	0.5
Compactness	0.7

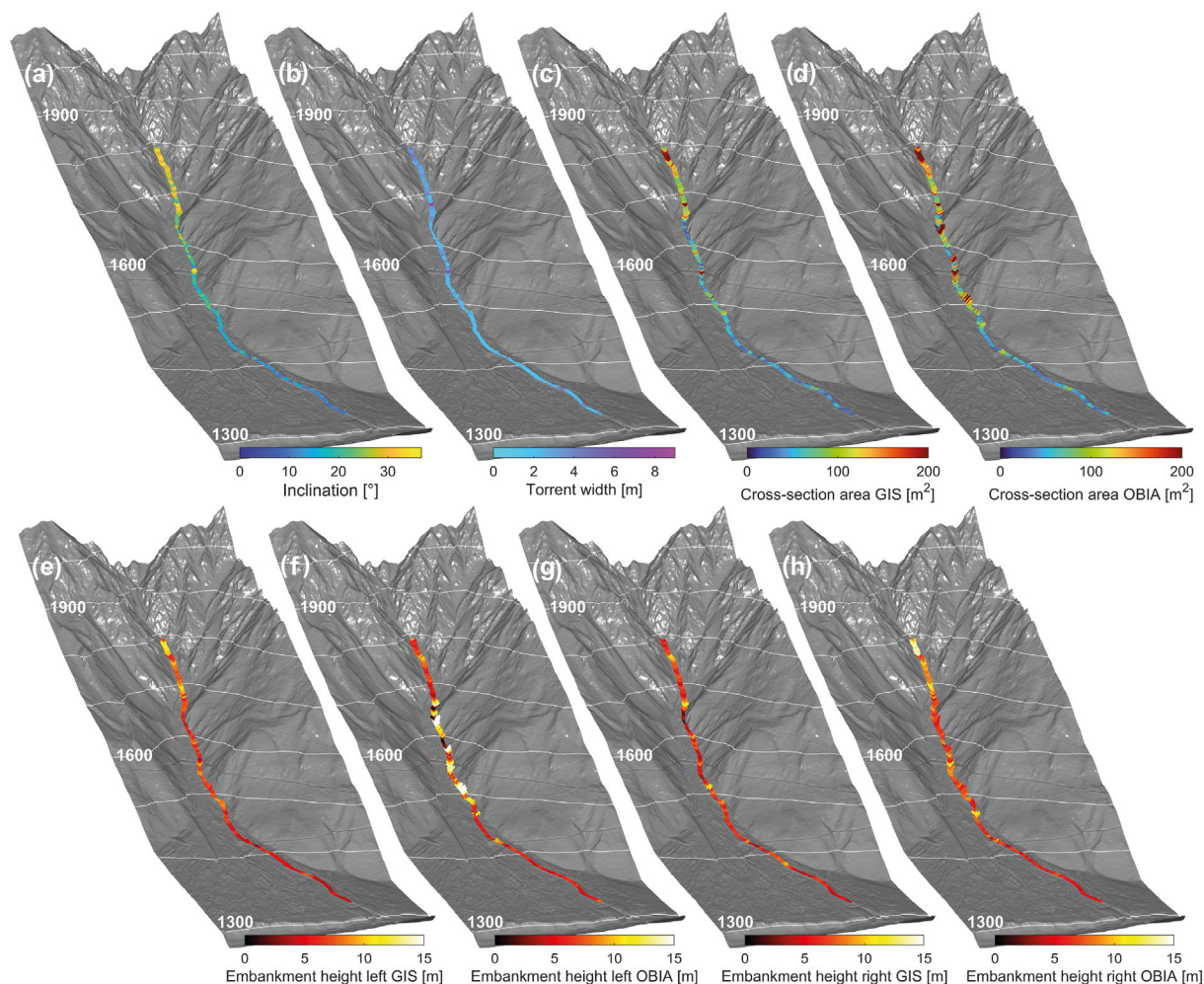
**TABLE B2** Criteria used to classify the torrential extent within eCognition.

Entity	Criteria
Mean slope	>10 and <90
Mean distance map	<30
10th percentile distance map	<12
90th percentile distance map	<90
Standard deviation distance map	<18

**APPENDIX C: FIGURES TORRENTIAL PROPERTIES**



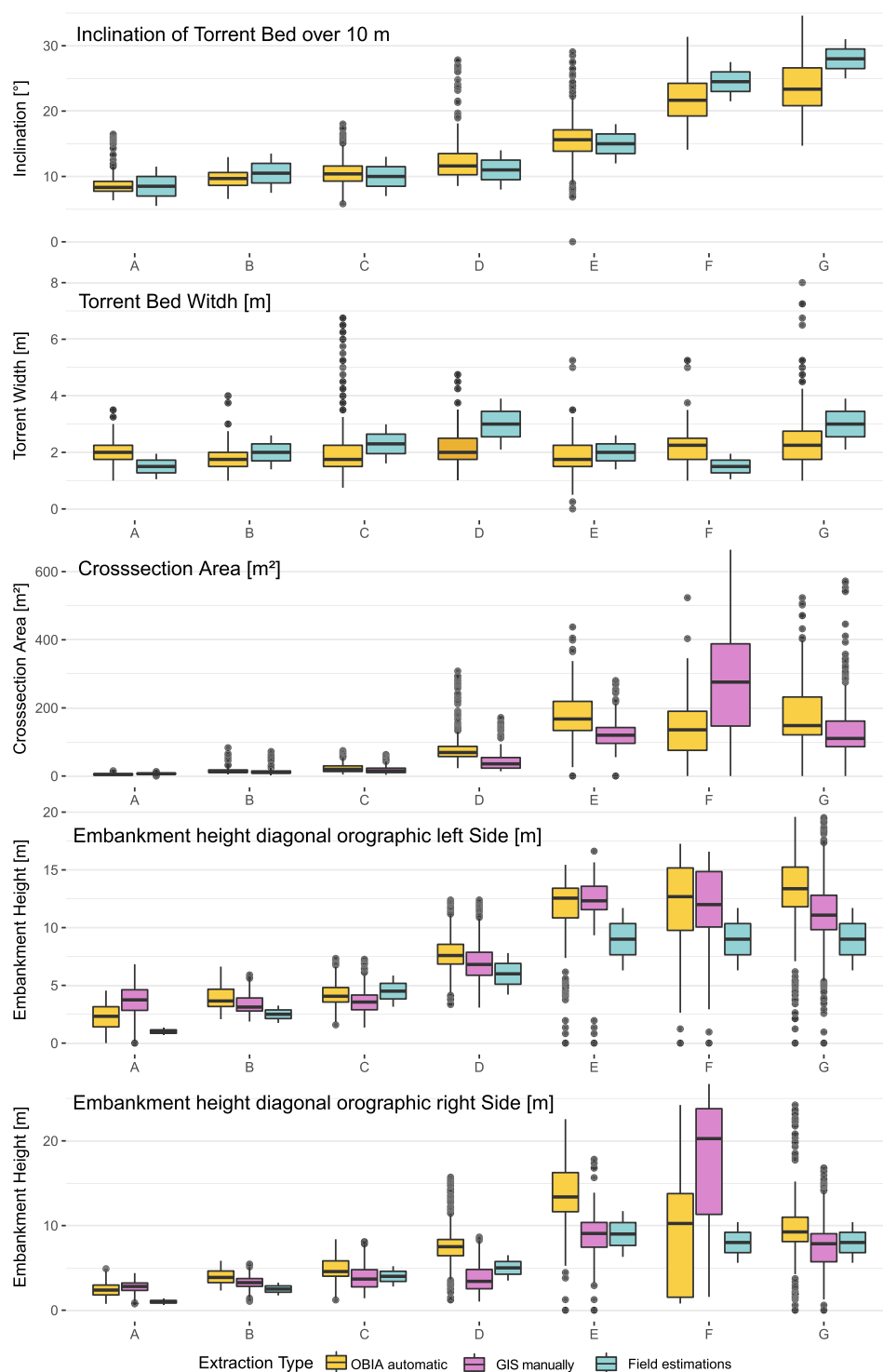
**FIGURE C1** Extracted torrential properties of Arelen: (a) inclination torrent bed, (b) torrent bed width, (c) cross-section area based on manually drawn embankment polygon in GIS, (d) cross-section area based on automatic OBIA, (e) embankment height left based on manually drawn embankment polygon in GIS, (f) embankment height right based on automatic OBIA, (g) embankment height right based on manually drawn embankment polygon in GIS and (h) embankment height left based on automatic OBIA [Color figure can be viewed at [wileyonlinelibrary.com](https://onlinelibrary.wiley.com/doi/10.1002/esp.5585)]



**FIGURE C2** Extracted torrential properties of Fraschmardin: (a) Inclination torrent bed, (b) torrent bed width, (c) cross-section area based on manually drawn embankment polygon in GIS, (d) cross-section area based on automatic OBIA, (e) embankment height left based on manually drawn embankment polygon in GIS, (f) embankment height right based on automatic OBIA, (g) embankment height right based on manually drawn embankment polygon in GIS and (h) embankment height right based on automatic OBIA [Color figure can be viewed at [wileyonlinelibrary.com](https://onlinelibrary.wiley.com/doi/10.1002/esp.5585)]



**FIGURE C3** Comparison of torrent characteristics of the Arelen catchment. The resulting values of torrent bed width and inclination are consistent along the field- and GIS-based extraction. Along the old debris-flow cone (sections A–D), the embankments extracted automatically with OBIA and manually with GIS and the derived crosssectional area are largely consistent. One of the uppermost section F on the embankment of the orographic right side has large discrepancies [Color figure can be viewed at [wileyonlinelibrary.com](https://onlinelibrary.wiley.com/doi/10.1002/esp.5585)]



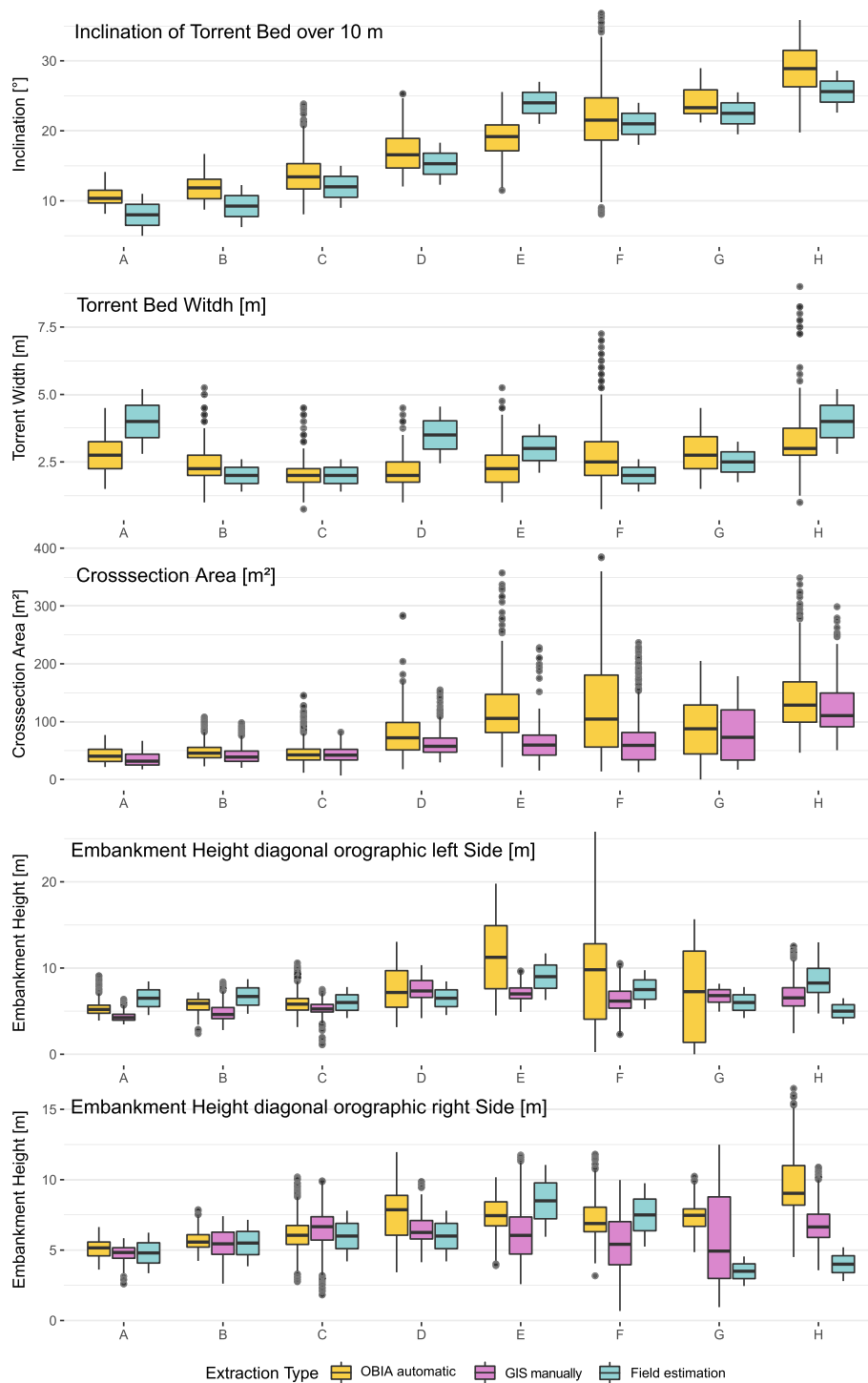


**FIGURE C4** Comparison of the torrent parameters of the Fraschmardin catchment. OBIA and manually extracted GIS values displayed according to their distribution, field measurements with their survey uncertainties, respectively. The resulting values of torrent bed width and inclination are consistent along the field- and GIS-based extraction. The OBIA-based embankment measurements show a particularly large variation along densely vegetated and landslide-prone areas [Color figure can be viewed at [wileyonlinelibrary.com](http://wileyonlinelibrary.com)]